The Catalan seismic crisis (1427 and 1428; NE Iberian Peninsula): Geological sources and earthquake triggering

Hector Perea

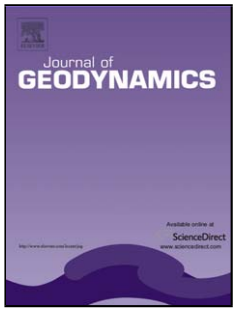

Title: The Catalan seismic crisis (1427 and 1428; NE Iberian Peninsula): Geological sources and earthquake triggering

Author: Hector Perea

PII: S0264-3707(09)00003-9
DOI: doi:10.1016/j.jog.2009.01.002
Reference: GEOD 874

To appear in: *Journal of Geodynamics*

Received date: 5-9-2008
Revised date: 9-1-2009
Accepted date: 11-1-2009

Please cite this article as: Perea, H., The Catalan seismic crisis (1427 and 1428; NE Iberian Peninsula): Geological sources and earthquake triggering, *Journal of Geodynamics* (2008), doi:10.1016/j.jog.2009.01.002

The Catalan seismic crisis (1427 and 1428; NE Iberian Peninsula): Geological sources and earthquake triggering

Hector Perea[1*]

[1] LATTEX-IDL, Dpt. de Geología, Fac. Ciências, Universidade de Lisboa, 1749-016 Lisboa, Portugal

[*] Corresponding author: hector.perea@fc.ul.pt Teleph (+351) 217500000 (ext. 26296) Fax (+351) 217500119

Abstract

The Catalan seismic crisis of the years 1427 and 1428 is one of the most destructive seismic episodes that happened in the northeastern Iberian Peninsula in historical times. The main earthquakes of this crisis occurred on March 19th 1427 in the zone around Amer (I_{EMS-98}=VIII), May 15th 1427 in the vicinity of Olot (I_{EMS-98}=VIII) and on February 2nd 1428 in the area close to Camprodon (I_{EMS-98}=IX). There is much evidence that the Amer fault produced the first two events of this crisis, but is still uncertain which fault generated the earthquake on February 2nd 1428. Using newly available macroseismic data, the earthquake area sources of the three main earthquakes of the crisis have been obtained and they corroborate that the Amer fault may be the origin of the first two events. However, the area source corresponding to the last earthquake of the crisis cannot

be associated to a single fault and indicates three possible candidates: the Vallfogona and Ribes-Camprodon thrusts and the Amer normal fault. Modeling of the Coulomb failure stress transfer has been performed to help determine the best candidate responsible for the February event. The results of the modeling points to: a) a triggering relationship between the three main events of the crisis and b) the Amer fault, or a similar extensional fault close and parallel to it, as the most probable origin of the earthquake on February 2nd 1428.

Key-words: Catalan seismic crisis; historical earthquakes; seismogenic faults; earthquake triggering; Coulomb failure stress transfer.

1- Introduction

To establish the faults that have produced big and potentially destructive earthquakes during the Quaternary and to predict where and, approximately, when the next one might occur are the main objectives of seismotectonic and active tectonic studies. One of the basic ways to localize active faults is to study large historical earthquakes reported on seismic catalogs. From the geographical relationship between the distribution of the damaged localities during one of these large earthquakes and the surrounding geological structure, it may be possible to identify the fault responsible for the event.

The Catalan seismic crisis constitutes the most destructive seismic episode that has taken place in the northeastern Iberian Peninsula (Fontserè and Iglésies, 1971; Cadiot, 1979;

Banda and Correig, 1984; Lambert, 1993; Olivera et al., 2006). The crisis occurred during the years 1427 and 1428 and the study of its three main shocks (figure1 and table 1), March 19th 1427 (I_{EMS-98}=VIII), May 15th 1427 (I_{EMS-98}=VIII) and February 2nd 1428 (I_{EMS-98}=IX), and the search for the fault or faults that produced them has been the objective of various studies (Fontserè and Iglésies, 1971; Banda and Correig, 1984; Briais et al., 1990; Ferrer et al., 1999; Fleta et al., 2001; Olivera et al., 2006; Perea, 2006; Perea et al., 2006). The identification of these faults and the recognition of the triggering relation between the main earthquakes may lead to an improvement of future seismic hazard studies performed in this region.

The objectives of the present work are: a) to assess the location and size of the area sources corresponding to the three main earthquakes of the Catalan seismic crisis, applying the method proposed by Gasperini et al. (1999) and using the new data published by Olivera et al. (2006); b) to try to identify the active faults that produced these earthquakes; and c) to perform a Coulomb failure stress transfer modeling to elucidate the influence of each of them in the occurrence of each other.

2- Seismotectonics of the northeastern Iberian Peninsula

The active faults located in intraplate regions, such as the northeastern Iberian Peninsula, show low strain rates. Although the seismicity in these regions is low and characterized by earthquakes of low to moderate magnitude, some big earthquakes have occurred in the past, such as those of the Catalan seismic crisis, and could be repeated in the future with

important economic and social consequences. Recent studies about the active tectonics of the northeastern Iberian Peninsula show that the slip rate of active faults ranges between 0.1 and 0.01 mm/yr and the mean recurrence interval of the big earthquakes lies between 10^3 and 10^5 years (Masana, 1995; Masana et al., 2001a; Masana et al., 2001b; Perea et al., 2003; Perea, 2006; Perea et al., 2006). Therefore, the existence of these active faults in low strain regions and its potentiality to produce big earthquakes bring out the necessity to include their study and analysis into seismic hazard projects.

The northeastern Iberian Peninsula is characterized by the interference between Paleogene compression structures related to the Pyrenees orogen (Muñoz et al., 1986; Vergés and Martinez, 1988; Pujadas et al., 1989; Muñoz, 1992; Muñoz, 2002) and Neogene extensional basins related to the opening of the western Mediterranean (Saula et al., 1996; Tassone et al., 1996; Doglioni et al., 1999; Jolivet et al., 1999; Lewis et al., 2000; Roca et al., 2001; Gelabert et al., 2002). The main Pyrenean structures are thrusts, and associated folds, which have an approximately E-W strike and which dip about 40º to the north (Muñoz et al., 1986). The Neogene extensional basins located in the study area are bounded by mountain fronts, the Transverse ranges, controlled by normal faults with an approximately NW-SE direction with the main ones dipping about 60º to the NE (Saula et al., 1996).

The instrumental seismicity in the northeastern Iberian Peninsula can be described as moderate to low, given the magnitude and the number of earthquakes (Olivera et al., 1992; Perea, 2006; Perea et al., 2006). The geographic distribution of the earthquakes

reveals that the Pyrenees and the Transverse ranges are characterized by a high density of events when compared with the whole area (figure 2a). Regarding the depth distribution of the earthquakes, the seismicity can be described as shallow since more than 90% of the events are located between the surface and 15-20 km depth (figure 2b). This depth approximately coincides with the location of the detachment of the main thrust and normal faults located in the zone. Thus, the active faults may be related to the Pyrenees and the Transverse ranges structures (Perea, 2006; Perea et al., 2006). Moreover, the seismogenic crust might correspond to the first 15-20 km of the crust, taking into account the depth range where the seismicity is mainly located. According to this, the fault rupture planes that will be used in the Coulomb failure stress transfer modeling must not surpass the 20 km depth, the bottom boundary of the seismogenic crust.

3- The Catalan seismic crises

The Catalan seismic crisis began at the end of February 1427 and lasted until August 1428 (Olivera et al., 2006). The first earthquakes were felt in the Girona bishopric at the end of February 1427. During the night between March 2nd and 3rd two earthquakes, that did not produced damage, were felt in Barcelona and in the entire Girona bishopric. Following this, on March 13th, 14th and 15th another three earthquakes struck the same zone, the largest being the one on the 13th (I_{EMS-98}=VI-VII) with its epicenter located close to the town of Amer (figure 1 and table 1). These three earthquakes already had produced damage and alarm in the population close to the epicentral area, who began to sleep in tents placed in fields next to the affected cities and towns.

116

117 The first big earthquake of the crisis occurred on March 19th 1427 (figure 1 and table 1).
118 This event produced significant damage in Amer and nearby towns, and was felt in the
119 majority of the Catalan territory and southern France. Olivera et al. (2006) assign to this
120 event a maximum intensity of VIII (EMS-98), a seismic moment (Mo) of 8.43*10^{17} Nm,
121 a moment magnitude (Mw) of 5.9 and a focal depth of 6 km, and locate the epicenter
122 slightly to the south of Amer. These authors obtained the Mo using the relationships
123 between this parameter and the area inside a given intensity contour (Johnston, 1996a;
124 Johnston, 1996b), the Mw by means of Hanks and Kanamori (1979) relationship and the
125 focal depth using the Sponheuer (1960) law.

126

127 After the March 19th earthquake, a series of aftershocks occurred in the vicinity of the
128 epicentral zone from March 21st until 22nd, and on April 13th, 22nd and 23rd (Olivera et al.,
129 2006). Among them, the largest was the one on April 22nd, with an assigned intensity of
130 VI-VII (EMS-98) and an epicenter located in the zone of Lloret Salvatge, slightly to the
131 north of Amer (figure 1 and table 1). This aftershock was the first event of the crisis that
132 produced casualties, caused by toxic gas emissions.

133

134 On May 15th 1427 the second big earthquake of the crisis occurred (Fontserè and Iglésies,
135 1971; Olivera et al., 2006). The zone between Olot and the Vall d'en Bas, which is
136 located about 20 km to the north of the area where the previous earthquakes had taken
137 place, was the most damaged (figure 1 and table 1). Olivera et al. (2006) assigned to this

earthquake an intensity of VIII (EMS-98), a Mo of $6.31*10^{17}$ Nm, a Mw of 5.8 and a focal depth of 5 km.

Between May 15th and June 4th 1427 small earthquakes where felt in the Girona bishopric (Olivera et al., 2006). After these, an event of intensity VI (EMS-98) occurred on June 8th and was followed by numerous tremors on June 12th, all of them close to the city of Girona. Following this, on June 14th an earthquake of intensity VII (EMS-98) produced the collapse of half of the town of Caldes de Malavella (figure 1 and table 1), 15 km to the south of the city of Girona. Olivera et al. (2006) assigned to this event a Mw of 5.3. Between June 15th 1427 and February 2nd 1428 several other earthquakes were felt in the vicinity of Girona, mainly between July and August, all of them with intensities lower than V (EMS-98).

The last of the big earthquakes of the Catalan seismic crisis occurred on February 2nd 1428 (Fontserè and Iglésies, 1971; Cadiot, 1979; Banda and Correig, 1984; Lambert, 1993; Olivera et al., 2006). This was the largest of the three main events of the crisis and its epicentral zone was located close to the town of Camprodon (I_{EMS-98}=IX; Olivera et al., 2006), approximately 15 km to the north of Olot (figure 1 and table 1). This earthquake produced significant damage in the proximity of the epicentral area, more than 1000 casualties and was felt in up to almost 300 km from the epicenter. Olivera et al. (2006) calculated a Mo of $5.95*10^{18}$ Nm, a Mw of 6.5 and a focal depth of 9 km.

After the earthquake on February 2nd 1428, there are no further data regarding the occurrence of aftershocks, probably eclipsed by the high magnitude and destruction of this last event (Olivera et al., 2006). It is known only that small earthquakes did occur during July and August 1428.

4- Earthquakes area sources and seismogenic faults

The historical reports describing the damage produced by a certain earthquake in different localities can be used to determine the fault that produced it. Gasperini et al. (1999) proposed a method ("Gasperini method" henceforth), which is based on algorithms developed in Gasperini and Ferrari (1995 and 1997), to assess the location, size and orientation of an earthquake area source using the distribution of the intensity data points, cities or sites where the earthquake caused damage or was felt. The final result of the method is an oriented rectangle that describes the earthquake area source and is meant to represent the surface projection of the fault responsible for the earthquake or the portion of the Earth where it would be likely to be located. The projection of the obtained earthquake area source on a geological map of the area could allow us to determine the fault that was the origin of the historical earthquake. Gasperini et al. (1999) obtained the source of some Italian historical earthquakes with magnitude equal or higher than 5.5, which means intensities equal or higher than VIII (Ambraseys, 1985; López Casado et al., 2000). Therefore, in this study the Gasperini method has been only applied to assess the source of the three main earthquakes of the Catalan seismic crisis (March

19th and May 15th 1427 and February 2nd 1428) using the intensity data points published by Olivera et al. (2006).

Olivera et al. (2006) furnished 49 localities where there is available information about the March 19th 1427 earthquake (22 with assigned intensity, figure 3a; 15 with supposed probable damages; 11 with a felt report; 1 with local effects). The data points with assigned maximum intensity (5 localities with I_{EMS-98}=VIII) are located around Amer. The earthquake area source obtained applying the Gasperini method has a NNW-SSE direction, a rupture area of 50.4 km^2 (8.0*6.3 km) that corresponds to a Mw of 5.7±0.4 earthquake and the epicenter is located to the south of Amer (figure 3a and source A in figure 4). When the location of the earthquake area source is projected onto a geological map it shows partial spatial superposition with the southern Amer fault (figure 4). This is an extensional fault located in the Transverse ranges with a NNW-SSE direction and dipping around 60º to the NE (Saula et al., 1996). Therefore, the southern Amer fault could be considered as the fault that generated the March 19th 1427 earthquake. This inference is supported by the conclusions that other authors have made from geomorphologic, geophysical and seismotectonic studies of the Amer fault (Goula et al., 1992; Ferrer et al., 1999; Fleta et al., 2001; Perea, 2006; Perea et al., 2006).

According to Olivera et al. (2006), the May 15th 1427 affected 38 localities (22 with assigned intensity, figure 3b; 5 with supposed probable damage; 10 with a felt report; 1 with local effects). The maximum intensity data points (6 localities with I_{EMS-98}=VIII) are located between Olot and the Vall d'en Bas valley, a basin to the west of Olot related to

the Amer fault. The Gasperini method gives an earthquake area source located in the Vall d'en Bas zone, with a NE-SW direction and a rupture area of approximately 38 km^2 (6.6*5.7 km) that corresponds to an earthquake of Mw 5.5±0.3 (figure 3b and source B in figure 4). As a result of projecting the earthquake area source on a geological map it could be concluded that the May 15th event was also produced by the Amer fault (figure 4). Although there is a discrepancy between the direction of the area source and the direction of the fault, the source is entirely located inside the hanging wall of the Amer fault, clearly pointing to this fault as the origin of the earthquake. In accordance with the area source location, this event was generated by a segment of the fault located to the north of the one that ruptured during the March 19th earthquake, close to where the fault changes its direction from NW-SE to NNW-SSE. The Amer fault being responsible for this earthquake is also supported by other studies (Goula et al., 1992; Ferrer et al., 1999; Fleta et al., 2001; Perea, 2006; Perea et al., 2006).

For the third and the strongest earthquake of the seismic crises, the February 2nd 1428, Olivera et al. (2006) furnished 136 localities with information about the event (70 with assigned intensity, figure 3c; 36 with damage reported; 27 with probable damage; and 3 with insufficient information). The maximum intensity was assigned to the town of Camprodon (I_{EMS-98}=IX), but around it there are 24 localities with an I_{EMS-98}=VIII-IX. The earthquake area source obtained applying the Gasperini method is located to the north of the May 15th event epicentral zone, has a WNW-ESE direction and a rupture area of approximately 164 km^2 (17.1*9.6 km), corresponding to an earthquake of Mw 6.2±0.3 (figure 3c and source C in figure 4). In contrast with the previous two analyzed events of

the crisis, the projection of the earthquake area source onto the geological map does not show an univocal spatial relationship with one fault. However, it permits three possible candidates: the Vallfogona and the Ribes-Camprodon thrusts and the northern zone of the Amer fault (figure 4). Although Briais et al. (1990) suggested the Tet fault as another possible source for this earthquake, the results here refute this given that the area source obtained does not reveal any kind of spatial relationship with this fault (figure 4).

5- Static stress transfer modeling

5.1 Coulomb failure stress transfer

When an earthquake occurs it changes the state of static stress in the surrounding crust. Studies of Coulomb failure stress transfer have shown that the occurrence of moderate to large earthquakes can trigger subsequent earthquakes and exerts some control on the distribution of the aftershocks and quiescent zones (Reasenberg and Simpson, 1992; King et al., 1994; Harris and Simpson, 1996; Hodgkinson et al., 1996; Nostro et al., 1997; Hardebeck et al., 1998; Harris, 1998; Harris and Simpson, 1998; Nalbant et al., 1998; Toda et al., 1998; Parsons et al., 1999; Harris, 2000; Wyss and Wiemer, 2000; Jacques et al., 2001; Lin and Stein, 2004; Martínez-Díaz et al., 2004; Ganas et al., 2005; Ganas et al., 2006; Martínez-Díaz et al., 2006; Nalbant et al., 2006; Parsons et al., 2006; Freed et al., 2007; Heidbach and Ben-Avraham, 2007). In this study, the objectives of the Coulomb stress transfer modeling have been: a) to establish the possible triggering relationships between the three main earthquakes of the Catalan seismic crisis; and b) to

identify the fault that generated the February 2nd 1428 event, poorly constrained by the Gasperini method.

The Coulomb failure stress change caused by the historical earthquakes has been calculated for dislocations in an elastic half-space (Okada, 1992) and on slip planes ("receiver faults" henceforth) with a given strike, dip and rake, or on receiver faults optimally oriented with respect to the regional stress field (Reasenberg and Simpson, 1992; King et al., 1994). The Coulomb failure stress change (ΔCFS) is given by: $\Delta CFS=\Delta\tau_c-\mu'\Delta\sigma_n$, where $\Delta\tau_c$ is the change in shear stress (positive in the direction of the fault slip), $\Delta\sigma_n$ is the change in normal stress (positive in unclamping of the fault) and μ' is the apparent friction coefficient of the fault. According to Nalbant et al. (1998) and taking into account that the majority of the faults located in the study area are normal faults, a value of 0.4 has been selected for μ'. Nevertheless, the variations of this parameter only modestly modify the Coulomb failure stress distribution around a fault (King et al., 1994; Nostro et al., 1997; Stein et al., 1997; Harris, 1998). A positive increase of the Coulomb failure stress transfer in an area is interpreted as meaning that a fault plane located in this area has been brought close to failure, whereas if it is negative the interpretation is the opposite (i.e., relaxed). For the modeling of the Coulomb failure stress transfer the Coulomb 3.1 software (Lin and Stein, 2004; Toda et al., 2005) has been used.

5.2 Present regional stress field

The Coulomb stress transfer modeling on optimally oriented receiver faults is most sensitive to the regional stress field orientation (King et al., 1994). Therefore, it is necessary to know the present regional stress field, which in northeastern Iberia has been evaluated using borehole breakout data (Jurado and Muller, 1997; Schindler et al., 1998) and focal mechanisms (Goula et al., 1999; Herraiz et al., 2000; de Vicente et al., 2008). However, the different studies show neither a single tectonic regime nor a homogeneous orientation of the stress field.

Jurado and Muller (1997) and Schindler et al. (1998) obtained from borehole breakout data that the maximum horizontal stress in the NE Iberian Peninsula has an orientation between NE-SW and ENE-WSW. The latter authors proposed a tectonic regime varying between extensional and stike-slip for the faults located on the north-western margin of the Valencia trough. Therefore, the maximum (σ_1) and intermediate (σ_2) stresses may be similar in magnitude, but clearly different from the minimum stress (σ_3) that is horizontal.

Goula et al. (1999) and Herraiz et al. (2000) evaluated the present stress field tensor from first P arrival focal mechanisms through the inversion method of Rivera and Cisternas (1990). The former authors obtained two solutions: a) a strike-slip stress tensor with a shape factor (defined as $Rs=(\sigma_2- \sigma_3)/(\sigma_1- \sigma_3)$) equal to 0.4 and a Q-score=0.854; and b) a compressive stress tensor with Rs=0.5 and Q-score=0.852. Both solutions have the compressive axis σ_1 in a sub-meridian position. The latter authors obtained, for the Pyrenees, a strike slip stress tensor solution with Rs=0.47, a Q-score=0.86, σ_1 being the maximum horizontal stress axis with an approximately N-S direction. Otherwise, these

297 authors, using the inversion method of Giner (1996), obtained for the eastern Pyrenees an
298 extensional stress tensor with σ_1 vertical and σ_3 with a NNE-SSW direction, a Rs=0.24
299 and a Q-score=0.98. Nevertheless, they also mention that the low number of events
300 analyzed (only four) diminishes the reliability of the results. Finally, de Vicente et al.
301 (2008) calculated the present stress tensor on the Iberian Peninsula from the inversion of
302 populations of moment tensor focal mechanisms. These authors obtained for the eastern
303 Pyrenees an extensional regime, with Rs=0.65 and σ_1=68/242 (dip and strike), σ_2=09/131
304 and σ_3=21/037.
305
306 The solution proposed by de Vicente et al. (2008) is only in agreement with the solution
307 proposed by Herraiz et al. (2000) using the inversion method of Giner (1996) and
308 different from those proposed by the other authors (Jurado and Muller, 1997; Schindler et
309 al., 1998; Goula et al., 1999; Herraiz et al., 2000). Whereas the latter authors propose a
310 maximum horizontal stress with a N-S to NE-SW direction and σ_1 or σ_2 being vertical,
311 the former ones propose σ_1 vertical, σ_2 with approximately NW-SE direction and σ_3 with
312 NE-SW direction.
313
314 In the Coulomb failure stress transfer modeling the stress tensor proposed by de Vicente
315 et al. (2008) for the Pyrenean zone will be used considering that: a) there is evidence of
316 Quaternary activity on normal faults located in the Pyrenees and surrounding zones, such
317 as the Lourdes fault (Alasset and Meghraoui, 2005), the Maladeta fault (Ortuño et al.,
318 2008) and the Amer fault (Perea et al., 2006; and the present study); and b) de Vicente et
319 al. (2008) conclude that the stress tensor solutions obtained by using the inversion of

moment tensor focal mechanisms show better quality compared to those obtained from first P arrival focal mechanisms.

5.3 Source and receiver faults

Source faults are defined as the fault planes that experiment displacement during the earthquake. Therefore, Coulomb stress transfer modeling has been performed considering as source faults the rupture planes corresponding to the March 19th and May 15th 1427 events, since the Amer fault is considered the responsible for both events, as stated above (figure 4). Two different possible source faults have been used for each earthquake in the modeling (figure 5), one using the information given by Olivera et al. (2006) (table 2a) and the other using the data obtained by applying the Gasperini method (table 2b). The characteristics of the source faults for each event are epicentral location, Mo, Mw, rupture area (RA), depth range and average displacement (table 2). When not available, the RA has been calculated using the empirical relationship between Mw and RA for normal faults proposed by Wells and Coppersmith (1994), the Mo has been obtained from the relationship between Mo and Mw and the average displacement has been established using the Mo expression, both from Hanks and Kanamori (1979) (table 2 for more details). The depth range has been established considering that both earthquakes are shallow (6 and 5 km depth respectively; Olivera et al, 2006), the dimensions of the source faults and the thickness of the seismogenic crust.

342 According to the distribution of the intensity data points furnished by Olivera et al.
343 (2006), and for the geographical location of the earthquake area sources obtained from
344 the Gasperini method, the source fault corresponding to the March 19th 1427 earthquake
345 is located close to the southern tip of the Amer fault. Following the same reasoning, the
346 event corresponding to the 15th May 1427 is located slightly to the north of the zone
347 where the fault changes direction from NW-SE to NNW-SSE (figure 5). Both source
348 faults are parallel to the strike of the Amer fault in each zone and dip 60º to the NE.
349
350 As mentioned above, the Coulomb failure stress transfer has been calculated on receiver
351 faults and the modification of their characteristics (strike, dip and rake) also changes the
352 pattern distribution of the stress lobes (Lin and Stein, 2004). In the modeling, the stress
353 change has been calculated on receiver faults optimally orientated with respect to the
354 present stress field, but also on particular receiver faults. In the second case, two different
355 directions and kinematics have been considered according to the faults observed in the
356 zone: a) receiver faults following the Pyrenean direction and kinematics, thrusts with an
357 approximate strike N90ºE and dipping around 40º towards the north, as the Vallfogona
358 and Ribes-Camprodon thrusts (Muñoz et al., 1986); and b) receiver faults following the
359 Transverse ranges direction and kinematics, normal faults with strike N145ºE and dipping
360 around 60º towards the northeast, as the Amer fault (Saula et al., 1996).
361
362 Considering the two different source faults and the three different receiver fault
363 geometries (optimally oriented and Pyrenees and Transverse ranges directions and
364 kinematics), six Coulomb stress transfer models were performed for the Catalan seismic

crisis (figures 6 and 7). The stress change was sampled at 6 km depth, taking into account the focal depths given by Olivera et al. (2006) for the March 19th and May 15th earthquakes, on a horizontal section of 125x100 km with 2.5x2.5 km grid spacing.

5.4 Results

The results of the Coulomb failure stress transfer modeling (figures 6 and 7) show that the location of the lobes where the stress increases and decreases are similar in relation to the source faults between models considering the same type of receiver faults. However, the size of the lobes are slightly different; the smallest dimensions are obtained when using the source faults deduced from the Gasperini method, clearly visible when results corresponding to the May 15th 1427 earthquake are compared (figures 6 and 7 second column). The models corresponding to the optimally oriented receiver faults (figures 6a and 7a) show that faults with directions approximately N120ºE, almost vertical (dipping between 80º to the SW and 90º) and with a rake implying mainly normal displacements (between -80º to -100º, following the Aki and Richards (1980) convention) are the best oriented with respect to the present stress field.

The Coulomb stress transfer results for the March 19th 1427 earthquake show that, when the receiver faults are normal faults (figures 6a/b and 7a/b first column), the maximum stress lobes are located to the north and south of the source fault. However, when the receiver faults are thrust faults (figures 6c and 7c first column) the lobes are situated in the area occupied by the source fault and two secondary maximums appear to the NE and

388 SW of it. Similar stress lobes distributions are observed for the May 15th 1427 earthquake
389 (figures 6 and 7 second column). Nevertheless, the models corresponding to the optimally
390 oriented faults (figures 6a and 7a second column) depict a third maximum stress lobe
391 close to the northeastern boundary of the source fault.
392
393 The pattern distribution of the stress lobes suggests that the May 15th earthquake was
394 strongly related to the occurrence of the March 19th event, which produces an increase of
395 Coulomb failure stress in normal faults with NW-SE direction to the north, in the vicinity
396 of the May earthquake source fault (figures 6a/b and 7a/b first column). This relationship
397 between both events is more clearly in the models using the source faults deduced from
398 Olivera et al. (2006) (figures 6a and b first column).
399
400 **6- Discussion: the source of the February 2nd 1428 earthquake**
401
402 According to the Coulomb failure stress modeling, the May 15th 1427 earthquake
403 produced an increase of the stress to the north and south of the source fault in normal
404 receiver faults with an approximately NW-SE direction (figure 8c) and around the source
405 fault in thrust receiver faults with E-W direction (figures 6c and 7c second column). But,
406 what was the fault responsible for the February 2nd 1428 earthquake? As mentioned
407 above, there are three possible candidates: the Vallfogona and the Ribes-Campordon
408 thrust faults, both with E-W direction, and the Amer normal fault, with approximately
409 NW-SE direction.
410

411 Taking into account the stress distribution and the probable triggering relation between
412 the main earthquakes of the crisis (figures 6c and 7c second column), the Ribes-
413 Camprodon thrust fault has little likelihood of being the source of the February 2nd 1428
414 event given the distance between it and the lobe of increased stress obtained when
415 considering E-W thrust receiver faults. Otherwise, considering the same evidence, the
416 Vallfogona thrust fault and the Amer normal fault are better candidates.
417
418 The occurrence of the May 15th 1427 earthquake produced an increase of the stress in E-
419 W thrust receiver faults in a zone where the Vallfogona thrust fault intersects the surface
420 (figures 6c and 7c second column), around 20 km to the south of the city of Camprodon,
421 pointing to this zone as a possible epicentral area. However, the results also show an
422 increase of the stress in normal receiver faults with NW-SE direction, such as the Amer
423 fault, to the north of the May event source fault (figure 8c). Furthermore, some results
424 show that, near the city of Camprodon, the increase of stress is significant and, thus,
425 indicating a favorable zone to locate a normal fault responsible of the final earthquake of
426 the crisis. The only normal fault known in the area to date is the Amer fault. Although it
427 seems not to have sufficient length to produce an earthquake of magnitude around 6.5, if
428 only its surface expression is considered, its subsurface continuation to the north or the
429 presence of another normal fault to the east but closeby cannot be discounted (Losantos et
430 al., 2002; Prof. Josep Mª Casas, Universitat de Barcelona, personal communication). It
431 seems more congruent to expect a normal fault as the source of this last event taking into
432 account that the two previous earthquakes of the crisis were generated by a fault with
433 such kinematics and considering the present stress field given by de Vicente et al. (2008).

Then, according to this, the Amer fault or some normal fault parallel to it would be the most probable source of the February 2nd 1428 earthquake, whereas the Vallfogona thrust fault would be a less probable source.

However, there are still important questions that should be answered: a) can the Amer fault rupture entirely in only one event or does the change in direction of the fault act as a boundary (barrier) between segments that rupture independently?; and b) if all the seismic crises related to the Amer fault followed the same behavior in the past, as described here, should we expect this to continue in the future? The answer to these questions will significantly improve the seismic hazard assessments in this area.

Finally, the Gasperini method has been of utility to localize the fault responsible of two large historical earthquakes in a zone of low strain rate. Moreover, the results obtained from applying this method have been helpful to define the dimensions and the geographical location of the source faults used in Coulomb failure stress transfer modeling. Although this method not always points to a unique fault as responsible of an historical earthquake as seen with the February 2nd 1428 event and as reported in other works (Perea, 2006; Perea et al., 2006), it has shown its potential to help researchers to localize the fault sources of large historical earthquakes in low strain zones or, at least, the probable area where this fault may be located and, also, that the information it gives is useful to other earthquake modeling studies.

7- Conclusions

This study corroborates that the Amer fault, in its southern and northern zones, would be the source of the first two main earthquakes of the Catalan seismic crisis, the March 19th and May 15th 1427 events. Also, the Coulomb failure stress transfer modeling points to a triggering relation between the three big earthquakes of the crisis.

It has not been possible to determine unequivocally the fault that generated the 2nd February 1428 earthquake. However, the results here discussed point to the Amer fault, or some other extensional fault parallel and close to it, as the most probable source of the event. The Vallfogona thrust has less probability to be the source of this event, but cannot be discarded. Finally, the Ribes-Camprodon thrust, still with some uncertainty, and the Tet fault have been discarded as possible fault sources.

Acknowledgements

The author is grateful to an anonymous reviewer, João Cabral, Josechu Martínez Díaz, Eulàlia Masana, Pere Santanach and Randell Stephenson for their comments and suggestions which significantly improve the manuscript. Hector Perea is sponsored by LATTEX/IDL-Fundação FCUL contract nº POCTI-ISFL-5-32 co-financed by FEDER. Some figures were prepared using the public domain Generic Mapping Tools GMT (Wessell and Smith, 1998).

References

Aki, K., Richards, P., 1980. Quantitative seismology, theory and methods. Freeman and Company, San Francisco, 948 pp.

Alasset, P.-J., Meghraoui, M., 2005. Active faulting in the western Pyrenees (France): Paleoseismic evidence for late Holocene ruptures. Tectonophysics, 409(1-4): 39-54.

Ambraseys, N., 1985. Intensity-attenuation and magnitude-intensity relationships for Northwest European earthquakes. Earthquake Eng.and Structural Dynamics, 13: 733-778.

Banda, E., Correig, A.M., 1984. The catalan earthquake of February 2, 1428. Engineering Geology, 20: 89-97.

Briais, A., Armijo, R., Winter, T., Tapponnier, P., Herbecq, A., 1990. Morphological evidence for Quaternary normal faulting and seismic hazard in the Eastern Pyrenees. Annales Tectonicae, 4(1): 19-42.

Cadiot, B., 1979. Les effets en France du séisme Catalan de 1428. In: J. Vogt (Editor), Les tremblements de terre en France. BRGM, Orleans, pp. 166-172.

de Vicente, G., Cloetingh, S., Munoz-Martin, A., Olaiz, A., Stich, D., Vegas, R., Galindo-Zaldivar, J., Fernandez-Lozano, J., 2008. Inversion of moment tensor focal mechanisms for active stresses around the microcontinent Iberia: Tectonic implications. Tectonics, 27(1).

Doglioni, C., Gueguen, E., Harabaglia, P., Mongelli, F., Durand, B., Jolivet, L., Horváth, F., Séranne, M., 1999. On the origin of the W-directed subduction zones and applications to the Western Mediterranean, The Mediterranean basins: Tertiary extension within the Alpine Orogene. Geological Society, London, Special Publications, 156, pp. 541-561.

502 Ferrer, P., Masana, E., Santanach, P., 1999. Expresión geomorfológica de la actividad
503 reciente de la falla de Amer (NE de la Península Ibérica). Acta Geol.Hispanica, 31(1996):
504 17-24.
505 Fleta, J., Santanach, P., Goula, X., Martínez, P., Grellet, B., Masana, E., 2001.
506 Preliminary geologic, geomorphologic and geophysical studies for the paleoseismological
507 analysis of the Amer fault (NE Spain). Netherlands Journal of Geosciences / Geologie en
508 Mijnbouw, 80(3-4): 243-253.
509 Fontserè, E., Iglésies, J., 1971. Recopilació de dades sísmiques de les terres catalanes
510 entre 1100 i 1906. Fundació Salvador Vives Casajuana, Barcelona, 548 pp.
511 Freed, A.M., Ali, S.T., Burgmann, R., 2007. Evolution of stress in Southern California
512 for the past 200 years from coseismic, postseismic and interseismic stress changes.
513 Geophysical Journal International, 169(3): 1164-1179.
514 Ganas, A., Shanov, S., Drakatos, G., Dobrev, N., Sboras, S., Tsimi, C., Frangov, G.,
515 Pavlides, S., 2005. Active fault segmentation in southwest Bulgaria and Coulomb stress
516 triggering of the 1904 earthquake sequence. Journal of Geodynamics, 40(2-3): 316-333.
517 Ganas, A., Sokos, E., Agalos, A., Leontakianakos, G., Pavlides, S., 2006. Coulomb stress
518 triggering of earthquakes along the Atalanti Fault, central Greece: Two April 1894 M6+
519 events and stress change patterns. Tectonophysics, 420(3-4): 357-369.
520 Gasperini, P., Bernardini, F., Valensise, G., Boschi, E., 1999. Defining seismogenic
521 sources from historical earthquake felt reports. Bulletin of the Seismological Society of
522 America, 89(1): 94-110.

523 Gasperini, P., Ferrari, G., 1995. Stima dei parametri sintetici. In: E. Boschi et al.
524 (Editors), Catalogo dei forti terremoti in Italia dal 461 a.C. al 1980. ING-SGA, Bologna,
525 pp. 96-111.
526 Gasperini, P., Ferrari, G., 1997. Stima dei parametri sintetici: nuove elaborazioni. In:
527 Boschi, E., Guidoboni, E., Ferrari, G., Valensise, G., Gasperini P. (Editors), Catalogo dei
528 forti terremoti in Italia dal 461 a.C. al 1990. ING-SGA, Bologna, pp. 56-64.
529 Gelabert, B., Sàbat, F., Rodríguez-Perea, A., 2002. A new proposal for the late Cenozoic
530 geodynamic evolution of the western Mediterranean. Terra Nova, 14: 93-100.
531 Giner, J., 1996. Análisis neotectónico y sismotectónico en el sector centro-oriental de la
532 cuenca del Tajo. Tesi doctoral Thesis, Univ. Complutense de Madrid, 345 pp.
533 Goula, X., Olivera, C., Escuer, J., Fleta, J., Grellet, B., Bousquet, J.C., 1992.
534 Neotectonics and seismicity of the area of the seismic crisis of 1427-28 in Catalonia.
535 Proceedings of the 22nd General Assembly of the European Seismological Comission,
536 Barcelona: 333-338.
537 Goula, X., Olivera, C., Fleta, J., Grellet, B., Lindo, R., Rivera, L.A., Cisternas, A.,
538 Carbon, D., 1999. Present and recent stress regime in the eastern part of the Pyrenees.
539 Tectonophysics, 308(4): 487-502.
540 Hanks, T., Kanamori, A., 1979. A moment magnitude scale. Journal of Geophysical
541 Research, 84: 2348-2350.
542 Hardebeck, J.L., Nazareth, J.J., Hauksson, E., 1998. The static stress change triggering
543 model: Constraints from two southern California aftershock sequences. Journal of
544 Geophysical Research-Solid Earth, 103(B10): 24427-24437.

545 Harris, R.A., 1998. Introduction to special section: Stress triggers, stress shadows, and
546 implications for seismic hazard. Journal of Geophysical Research, 103: 347-358.
547 Harris, R.A., 2000. Earthquake stress triggers, stress shadows, and seismic hazard.
548 Current Science, 79(9): 1215-1225.
549 Harris, R.A., Simpson, R.W., 1996. In the shadow of 1857 - The effect of the great Ft
550 Tejon earthquake on subsequent earthquakes in southern California. Geophysical
551 Research Letters, 23(3): 229-232.
552 Harris, R.A., Simpson, R.W., 1998. Suppression of large earthquakes by stress shadows:
553 A comparison of Coulomb and rate-and-state failure. Journal of Geophysical Research-
554 Solid Earth, 103(B10): 24439-24451.
555 Heidbach, O., Ben-Avraham, Z., 2007. Stress evolution and seismic hazard of the Dead
556 Sea Fault System. Earth and Planetary Science Letters, 257(1-2): 299-312.
557 Herraiz, M., De Vicente, G., Lindo-Naupari, R., Giner, J., Simon, J.L., Gonzalez-Casado,
558 J.M., Vadillo, O., Rodriguez-Pascua, M.A., Cicuendez, J.I., Casas, A., Cabanas, L.,
559 Rincon, P., Cortes, A.L., Ramirez, M., Lucini, M., 2000. The recent (upper Miocene to
560 Quaternary) and present tectonic stress distributions in the Iberian Peninsula. Tectonics,
561 19(4): 762-786.
562 Hodgkinson, K.M., Stein, R.S., King, G.C.P., 1996. The 1954 rainbow Mountain-
563 Fairview Peak-Dixie Valley earthquakes: A triggered normal faulting sequence. Journal
564 of Geophysical Research-Solid Earth, 101(B11): 25459-25471.
565 Jacques, E., Monaco, C., Tapponnier, P., Tortorici, L., Winter, T., 2001. Faulting and
566 earthquake triggering during the 1783 Calabria seismic sequence, pp. 499-516.

567 Johnston, A.C., 1996a. Seismic moment assessment of earthquakes in stable continental
568 regions .1. Instrumental seismicity. Geophysical Journal International, 124(2): 381-414.
569 Johnston, A.C., 1996b. Seismic moment assessment of earthquakes in stable continental
570 regions .2. Historical seismicity. Geophysical Journal International, 125(3): 639-678.
571 Jolivet, L., Frizon de Lamotte, D., Mascle, A., Séranne, M., Durand, B., Jolivet, L.,
572 Horváth, F., Séranne, M., 1999. The Mediterranean basins: Tertiary extension within the
573 Alpine Orogene - An introduction, The Mediterranean basins: Tertiary extension within
574 the Alpine Orogene, pp. 1-14.
575 Jurado, M.J., Muller, B., 1997. Contemporary tectonic stress in northeastern Iberia. New
576 results from borehole breakout analysis. Tectonophysics, 282(1-4): 99-115.
577 King, G.C.P., Stein, R.S., Lin, J., 1994. Static stress changes and the triggering of
578 earthquakes. Bull.Seism.Soc.Am., 84(3): 935-953.
579 Lambert, J., 1993. The Catalonian (1428) and Alpine (1564, 1644) earthquakes: review of
580 research in France. In: M. Stucchi (Editor), Historical investigation of european
581 earthquakes. CNR, Milano, pp. 145-159.
582 Lewis, C.J., Vergés, J., Marzo, M., 2000. High mountains in zone of extended crust:
583 Insights into the Neogene-Quaternary topographic development of the northeastern
584 Iberia. Tectonics, 19: 86-102.
585 Lin, J., Stein, R.S., 2004. Stress triggering in thrust and subduction earthquakes and stress
586 interaction between the southern San Andreas and nearby thrust and strike-slip faults -
587 art. no. B02303. Journal of Geophysical Research-Solid Earth, 109(B2): 2303-2303.
588 López Casado, C., Molina, S., Giner, J., Delgaco, J., 2000. Magnitude-intensity
589 relationship in the Ibro-Magrebian region. Natural Hazards, 22: 271-297.

590 Losantos, M., Aragonès, E., Berástegui, X., Palau, J., Puigdefàbregas, C., Soler, M.,
591 2002. Mapa geològic de Catalunya 1:250000 (2ª Ed.). Institut Cartogràfic de Catalunya.
592 Generalitat de Catalunya.
593 Martínez-Díaz, J.J., Alvarez-Gomez, J.A., Benito, B., Hernandez, D., 2004. Triggering of
594 destructive earthquakes in El Salvador. Geology, 32(1): 65-68.
595 Martínez-Díaz, J.J., Capote, R., Tsige, M., Villamor, P., Martin-Gonzalez, F., Insua-
596 Arevalo, J.M., 2006. Seismic triggering in a stable continental area: The Lugo 1995-1997
597 seismic sequences (NW Spain). Journal of Geodynamics, 41(4): 440-449.
598 Masana, E., 1995. L'activitat neotectònica a les Cadenes Costaneres Catalanes. tesi
599 doctoral Thesis, Universitat de Barcelona, 444 pp.
600 Masana, E., Villamarín, J.A., Sánchez-Cabañero, J.G., Plaza, J., Santanach, P., 2001a.
601 Seismogenic faulting in an area of low seismic activity: Paleoseismicity of the El Camp
602 fault (Northeast Spain). Netherlands Journal of Geosciences / Geologie en Mijnbouw,
603 80(3-4): 229-241.
604 Masana, E., Villamarín, J.A., Santanach, P., 2001b. Paleoseismic results form multiple
605 trenching analysis along a silent fault: The El Camp fault (Tarragona, northeastern
606 Iberian Peninsula). Acta Geológica Hispánica, 36(3-4): 329-354.
607 Muñoz, J.A., 1992. Evolution of the continental collision belt: ECORS-Pyrenees crustal
608 balanced corss-section. In: McClay, K.R. (Editor), Thrust tectonics. Chapman and Hall,
609 pp. 235-246.
610 Muñoz, J.A., 2002. Alpine tectonic I: the Alpine sustem north of the Betic Cordillera.
611 Tectonic setting; The Pyrenees. In: Gibbons, W., Moreno, T. (Editors), The geology in
612 Spain. Geological Society (London), pp. 370-385.

613 Muñoz, J.A., Martinez, A., Verges, J., 1986. Thrust sequences in the eastern Spanish
614 Pyrenees. Journal of Structural Geology, 8(3-4): 399-405.
615 Nalbant, S.S., Hubert, A., King, G.C.P., 1998. Stress coupling between earthquakes in
616 northwest Turkey and the north Aegean Sea. Journal of Geophysical Research-Solid
617 Earth, 103(B10): 24469-24486.
618 Nalbant, S.S., Steacy, S., McCloskey, J., 2006. Stress transfer relations among the
619 earthquakes that occurred in Kerman province, southern Iran since 1981. Geophysical
620 Journal International, 167: 309-318.
621 Nostro, C., Cocco, M., Belardinelli, M.E., 1997. Static stress changes in extensional
622 regimes: An application to southern Apennines (Italy). Bulletin of the Seismological
623 Society of America, 87(1): 234-248.
624 Okada, Y., 1992. Internal Deformation Due to Shear and Tensile Faults in a Half-Space.
625 Bulletin of the Seismological Society of America, 82(2): 1018-1040.
626 Olivera, C., Redondo, E., Lambert, J., Riera Melis, A., Roca, A., 2006. Els terratrèmols
627 dels segles XIV i XV a Catalunya. Monografies nº 30. Institur Cartogràfic de Catalunya,
628 Barcelona, 407 pp.
629 Olivera, C., Susagna, T., Roca, A., Goula, X., 1992. Seismicity of the Valencia trough
630 and surrounding areas. Tectonophysics, 203: 99-109.
631 Ortuño, M., Queralt, P., Martí, A., Ledo, J., Masana, E., Perea, H., Santanach, P., 2008.
632 The North Maladeta Fault (Spanish Central Pyrenees) as the Vielha 1923 earthquake
633 seismic source: Recent activity revealed by geomorphological and geophysical research.
634 Tectonophysics, 453(1-4): 246-262.

635 Parsons, T., Stein, R.S., Simpson, R.W., Reasenberg, P.A., 1999. Stress sensitivity of
636 fault seismicity: A comparison between limited-offset oblique and major strike-slip
637 faults. Journal of Geophysical Research-Solid Earth, 104(B9): 20183-20202.
638 Parsons, T., Yeats, R.S., Yagi, Y., Hussain, A., 2006. Static stress change from the 8
639 October, 2005 M=7.6 Kashmir earthquake. Geophysical Research Letters, 33(6): L06304.
640 Perea, H., 2006. Falles actives i perillositat sísmica al marge nord-occidental del solc de
641 València, PhD Thesis Universitat de Barcelona, Barcelona, 382 pp.
642 Perea, H., Figueiredo, P.M., Carner, J., Gambini, S., Boydell, K., participants in the
643 Europaleos, 2003. Paleosismological data from a new trench across the El Camp Fault
644 (Catalan Coastal Ranges, NE Iberian Peninsula). Annals of Geophysics, 46(5): 763-774.
645 Perea, H., Masana, E., Santanach, P., 2006. A pragmatic approach to seismic parameters
646 in a region with low seismicity: The case of eastern Iberia. Natural Hazards, 39(3): 451-
647 477.
648 Pujadas, J., Casas, J.M., Muñoz, J.A., Sàbat, F., 1989. Thrust tectonics and paleogene
649 syntectonic sedimentation in the Empordà area, sputheastern Pyrenees. Geodinamica
650 Acta, 3(3): 195-206.
651 Reasenberg, P.A., Simpson, R.W., 1992. Response of Regional Seismicity to the Static
652 Stress Change Produced by the Loma-Prieta Earthquake. Science, 255(5052): 1687-1690.
653 Rivera, L., Cisternas, A., 1990. Stress tensor and fault plane solutions for a population of
654 earthquake. Bull.Seism.Soc.Am., 80(3): 600-614.
655 Roca, E., Ziegler, P.A., Cavazza, W., Robertson, A.H.F., Crasquin-Soleau, S., 2001. The
656 northwestern mediterranean basin (Valencia trough, Gulf of Lions and Liguro-Provençal

657 basins): Structure and geodynamic evolution, Peri-Tethys Memoir 6: Peri-Tethyan rift -
658 Wrench basins and passive margins. Mem.Mus.National Hist.Nat., 186, pp. 671-706.
659 Saula, E., Picart, J., Mató, E., Llenas, M., Losantos, M., Berástegui, X., Agustí, J., 1996.
660 Evolución geodinámica de la fosa del Empordà y las Sierras Transversales. Acta
661 Geol.Hispánica, 29(2-4 (1994)): 55-75.
662 Schindler, A., Jurado, M.J., Muller, B., 1998. Stress orientation and tectonic regime in the
663 northwestern Valencia Trough from borehole data. Tectonophysics, 300(1-4): 63-77.
664 Sponheuer, W., 1960. Methoden zur Herdtiefenbestimmung in der makroseismik /
665 Freiberger Forschungshefte, C88. Akademie Verlag, Berlin, 120 pp.
666 Stein, R.S., Barka, A.A., Dieterich, J.H., 1997. Progressive failure on the North Anatolian
667 fault since 1939 by earthquake stress triggering. Geophysical Journal International,
668 128(3): 594-604.
669 Tassone, A., Roca, E., Muñoz, J.A., Cabrera, L., Canals, M., 1996. Evolución del sector
670 septentrional del margen continental catalán durante el Cenozoico. Acta Geol.Hispánica,
671 29(2-4): 3-37.
672 Toda, S., Stein, R.S., Reasenberg, P.A., Dieterich, J.H., Yoshida, A., 1998. Stress
673 transferred by the 1995 M-w = 6.9 Kobe, Japan, shock: Effect on aftershocks and future
674 earthquake probabilities. Journal of Geophysical Research-Solid Earth, 103(B10): 24543-
675 24565.
676 Toda, S., Stein, R.S., Richards-Dinger, K., Bozkurt, S.B., 2005. Forecasting the evolution
677 of seismicity in southern California: Animations built on earthquake stress transfer.
678 Journal of Geophysical Research-Solid Earth, 110(B5).

679 Vergés, J., Martinez, A., 1988. Corte compensado del Pirineo oriental: geometría de las
680 cuencas de antepaís y edades de emplazamiento de los mantos de corrimiento.
681 Act.Geol.Hisp., 23(2): 95-106.
682 Wells, D.L., Coppersmith, K.J., 1994. New empirical relationships among magnitude,
683 rupture length, rupture width, rupture area, and surface displacement.
684 Bull.Seism.Soc.Am., 84(4): 974-1002.
685 Wessell, P., Smith, W., 1998. New, improved version of the generic mapping tools
686 released. EOS Trans American Geophysical Union, 79(47): 579.
687 Wyss, M., Wiemer, S., 2000. Change in the probability for earthquakes in southern
688 California due to the Landers magnitude 7.3 earthquake. Science, 290(5495): 1334-1338.
689

690 **Figure captions**

691

692 Figure 1. Schematic geological map of the northeastern Iberian Peninsula with the
693 location of the macroseismic epicenters of the main earthquakes of the Catalan seismic
694 crisis (Olivera et al., 2006). Cities/towns: A: Amer; C: Camprodon; CM: Caldes de
695 Malavella; G: Girona; O: Olot. Mountain ranges and faults (italics): AF: Amer normal
696 fault; CCR: Catalan Coastal Ranges; RCT: Ribes-Camprodon thrust; TF: Tet normal
697 fault; TR: Transverse Ranges; VT: Vallfogona thrust.

698

699 Figure 2. Geographical distribution and depth of the instrumental seismicity registered in
700 the northeastern Iberian Peninsula (from Intituto Geográfico Nacional earthquake
701 catalogue between 1900 and 2003). a) Map showing the geographical distribution of the
702 earthquakes; color indicates their focal depth and the circle size their magnitude (m_{bLg}).
703 b) Profile a-a' showing the earthquakes focal depth; the projected earthquakes are located
704 until 50 km to both sides of the profile; the circle size is not related with the earthquake
705 magnitude. Co: Coastline; Py: Pyrenees; TR: Transverse ranges; VT: València trough.

706

707 Figure 3. Maps showing the distribution of the intensity data points and the intensity
708 contours (Olivera et al., 2006) corresponding to the: a) March 19th 1427 earthquake
709 located in the vicinity of the town of Amer; contours corresponding to I_{EMS-98} VIII and
710 VII; b) May 15th 1427 earthquake occurred in the vicinity of the town of Olot; contours
711 corresponding to I_{EMS-98} VIII and VII; and c) February 2nd 1428 earthquake that affected
712 the town of Camprodon and surrounding areas; contours corresponding to I_{EMS-98} VIII,

713 VII, VI and V. Cities/towns: A: Amer; B: Barcelona; C: Camprodon; G: Girona; L:
714 Lleida; N: Narbonne; O: Olot; P: Puigcerdà; Pe: Perpinyà; T: Tarragona; To: Toulouse.
715 Faults (italics): AF: Amer normal fault; RCT: Ribes-Camprodon thrust; TF: Tet normal
716 fault; VT: Vallfogona thrust.
717
718 Figure 4. Geological map of the northwestern Iberian Peninsula showing the location of
719 the earthquake source area of the main events of the Catalan seismic crises. Earthquake
720 source areas: A: March 19th 1427; B: May 15th 1427; C: February 2nd 1428. The map is in
721 UTM coordinate system zone 31 northern hemisphere.
722
723 Figure 5. Map showing the geographical location and the dimensions of the source faults
724 used in the Coulomb failure stress transfer modeling. For more information about the
725 source faults see Table 2 and text. Cities/towns: A: Amer; C: Camprodon; G: Girona; O:
726 Olot. Faults (italics): AF: Amer normal fault; RCT: Ribes-Camprodon thrust; VT:
727 Vallfogona thrust.
728
729 Figure 6. Maps showing the Coloumb failure stress changes at 6 km depth when using the
730 earthquake source faults deduced from Olivera et al. (2006) data. Maps in the first
731 column correspond to the stress change after the March 19th 1427 and maps in the second
732 to the cumulative stress change after March 19th and May 15th 1427 earthquakes. a)
733 Optimally oriented receiver faults; b) receiver faults following the direction of the
734 Transverse ranges (N145ºE and normal faults); and c) receiver faults following the
735 Pyrenean trend (N90ºE and thrust faults). See text for more information. Faults: AF:

736 Amer normal fault; RCT: Ribes-Camprodon thrust; TF: Tet normal fault; VT: Vallfogona
737 thrust.
738
739 Figure 7. Maps showing the Coloumb failure stress changes at 6 km depth when using the
740 earthquakes source faults deduced from the Gasperini method. Maps in the first column
741 correspond to the stress change after the March 19th 1427 and maps in the second to the
742 cumulative stress change after March 19th and May 15th 1427 earthquakes. a) Optimally
743 oriented receiver faults; b) receiver faults following the direction of the Transverse ranges
744 (N145ºE and normal faults); and c) receiver faults following the Pyrenean trend (N90ºE
745 and thrust faults). See text for more information. Faults: AF: Amer normal fault; RCT:
746 Ribes-Camprodon thrust; TF: Tet normal fault; VT: Vallfogona thrust.
747
748 Figure 8. Maps showing the Coulomb failure stress change at 6 km depth in different
749 periods of the Catalan seismic crisis. The earthquakes source faults correspond to those
750 deduced from the Olivera et al. (2006) data and the receiver faults are those following the
751 direction of the Transverse ranges (N145ºE and normal faults). a) Map with the location
752 of the March 13th 1427 earthquake macroseismic epicenter, the zone where the seismic
753 crisis began. b) Map with the location of the March 19th 1427 earthquake macroseismic
754 epicenter and the Coulomb failure stress change distribution. c) Map with the location of
755 the May 15th 1427 and February 2nd 1428 earthquakes macroseismic epicenters and the
756 Coulomb stress change distribution corresponding to the occurrence of the March and
757 May events. Cities/towns: A: Amer; C: Camprodon; CM: Caldes de Malavella; G:

758 Girona; O: Olot. Faults (italics): AF: Amer normal fault; RCT: Ribes-Camprodon thrust;
759 TF: Tet normal fault; VT: Vallfogona thrust.
760
761
762 **Table captions**
763
764 Table 1. The earthquakes of the Catalan seismic crisis with an assigned magnitude (Mw)
765 higher than 5.0 (Olivera et al., 2006).
766
767 Table 2. Parameters of the source faults used in the Coloumb failure stress transfer
768 modeling and corresponding to the March 19th and May 15th 1427 events. a) Source faults
769 deduced from Olivera et al. (2006) data; and b) source faults deduced from Gasperini
770 method.

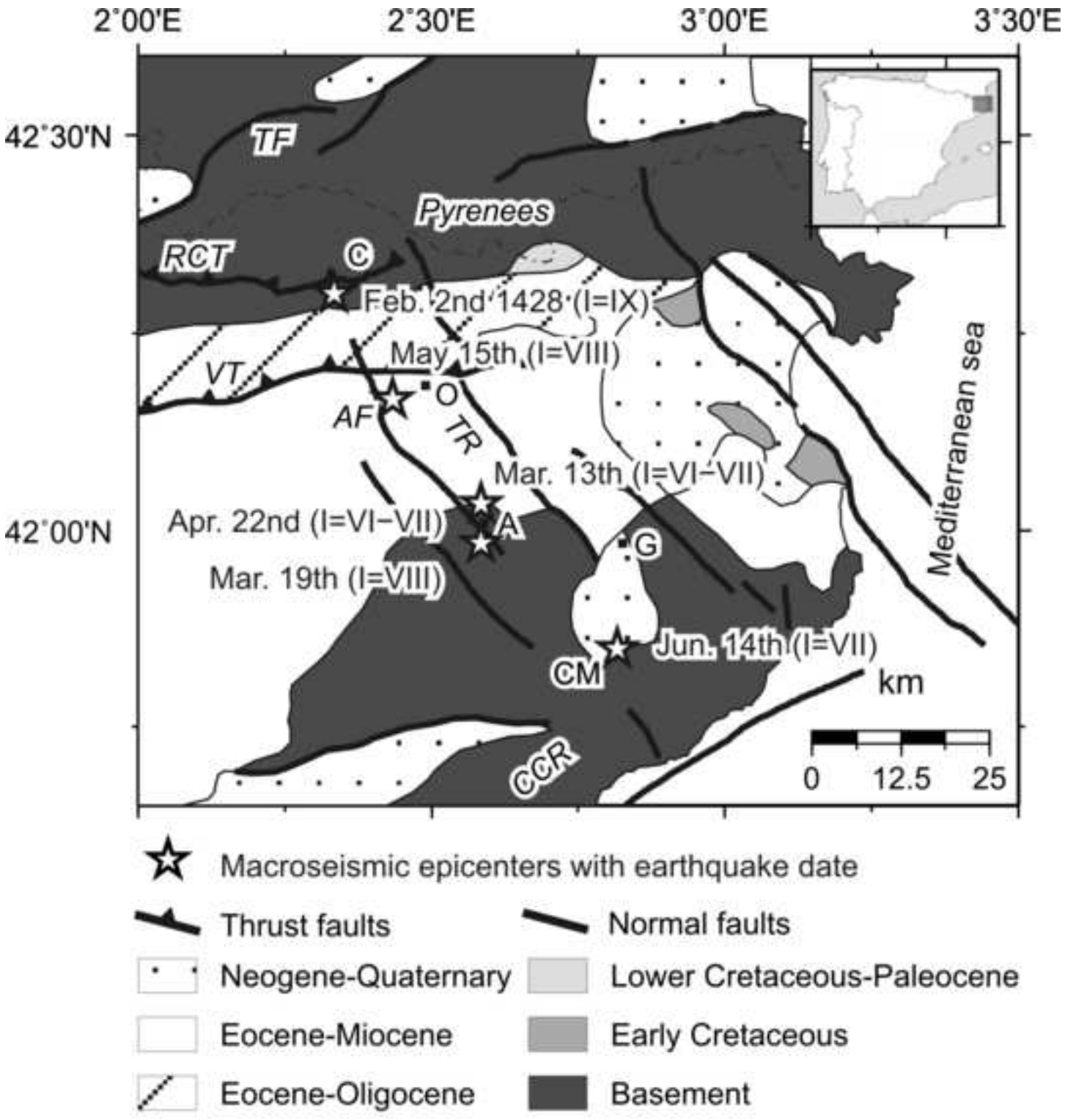

Figure 1 (Press publication)

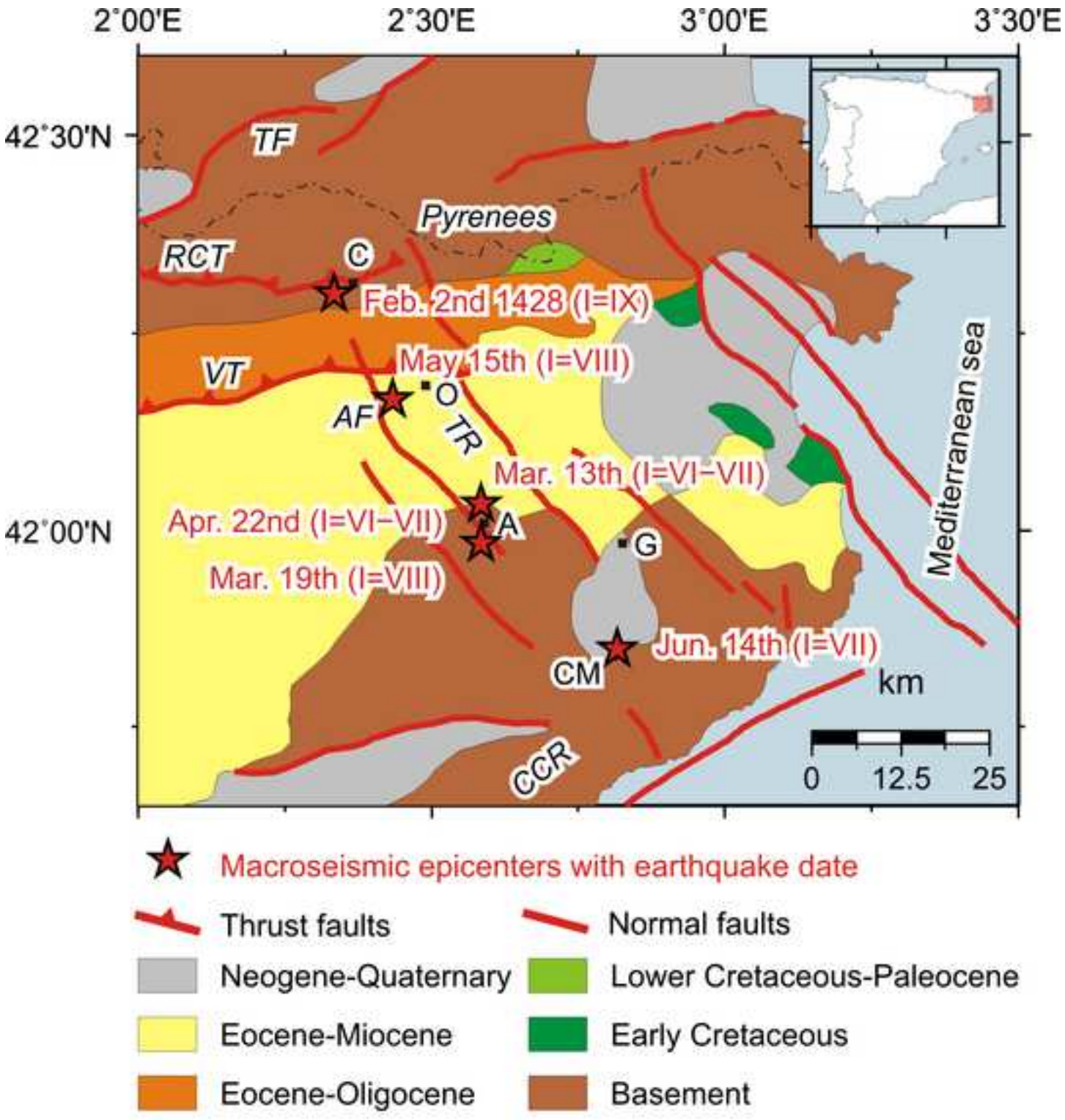

Figure 1 (Online publication)

Figure 2 Black&White
Click here to download high resolution image

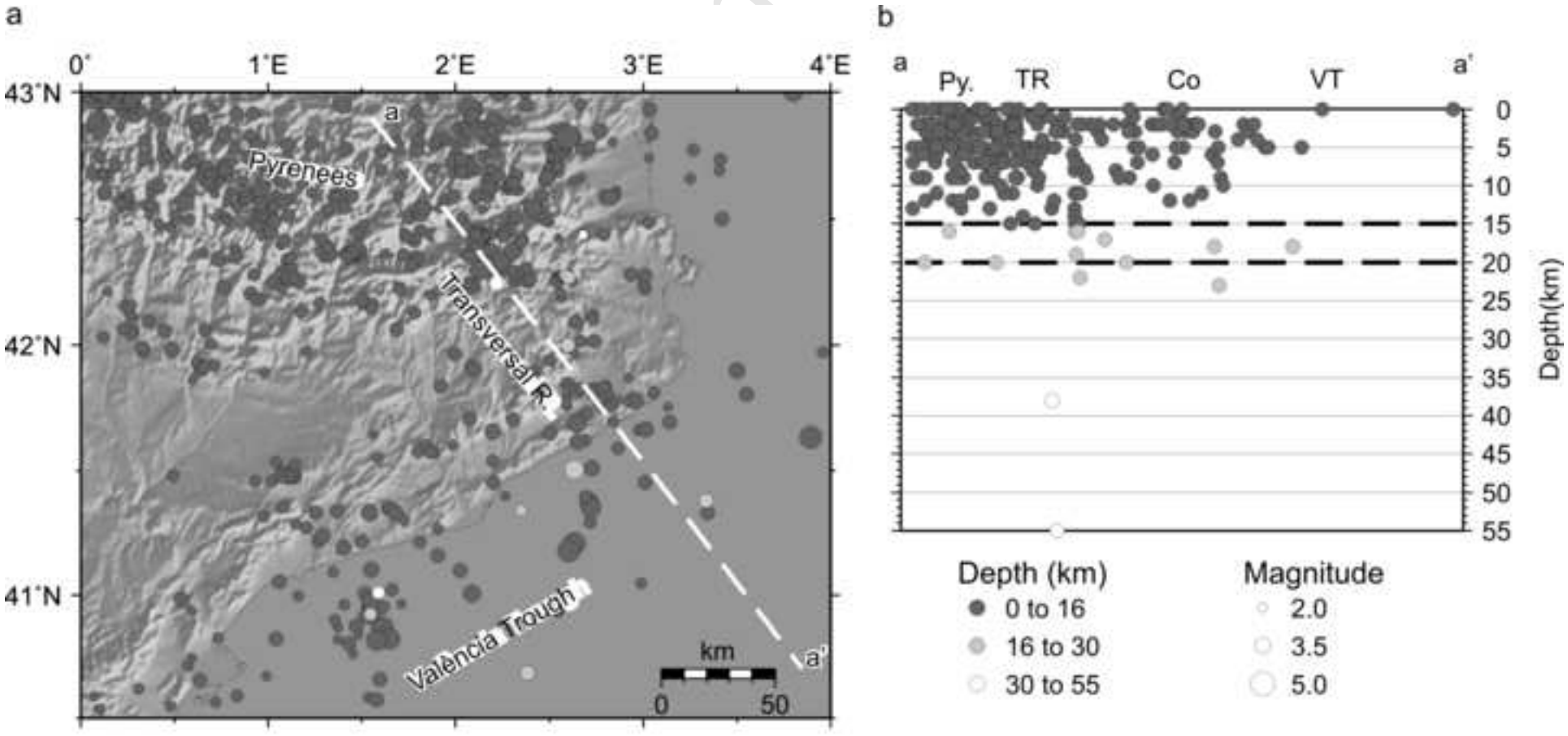

Figure 2 (press publication)

Figure 2 Color
Click here to download high resolution image

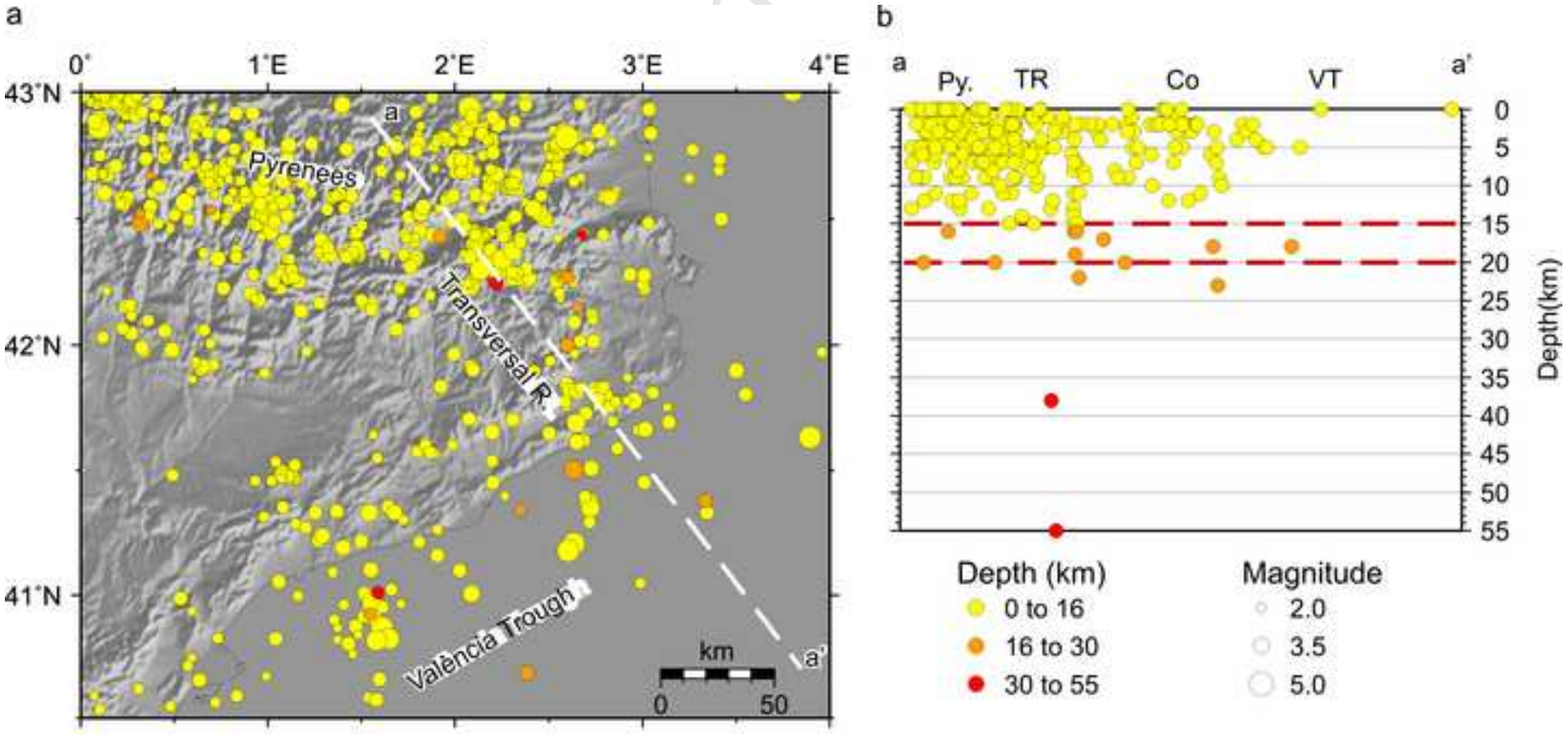

Figure 2 (online publication)

Figure 3 Black&White
Click here to download high resolution image

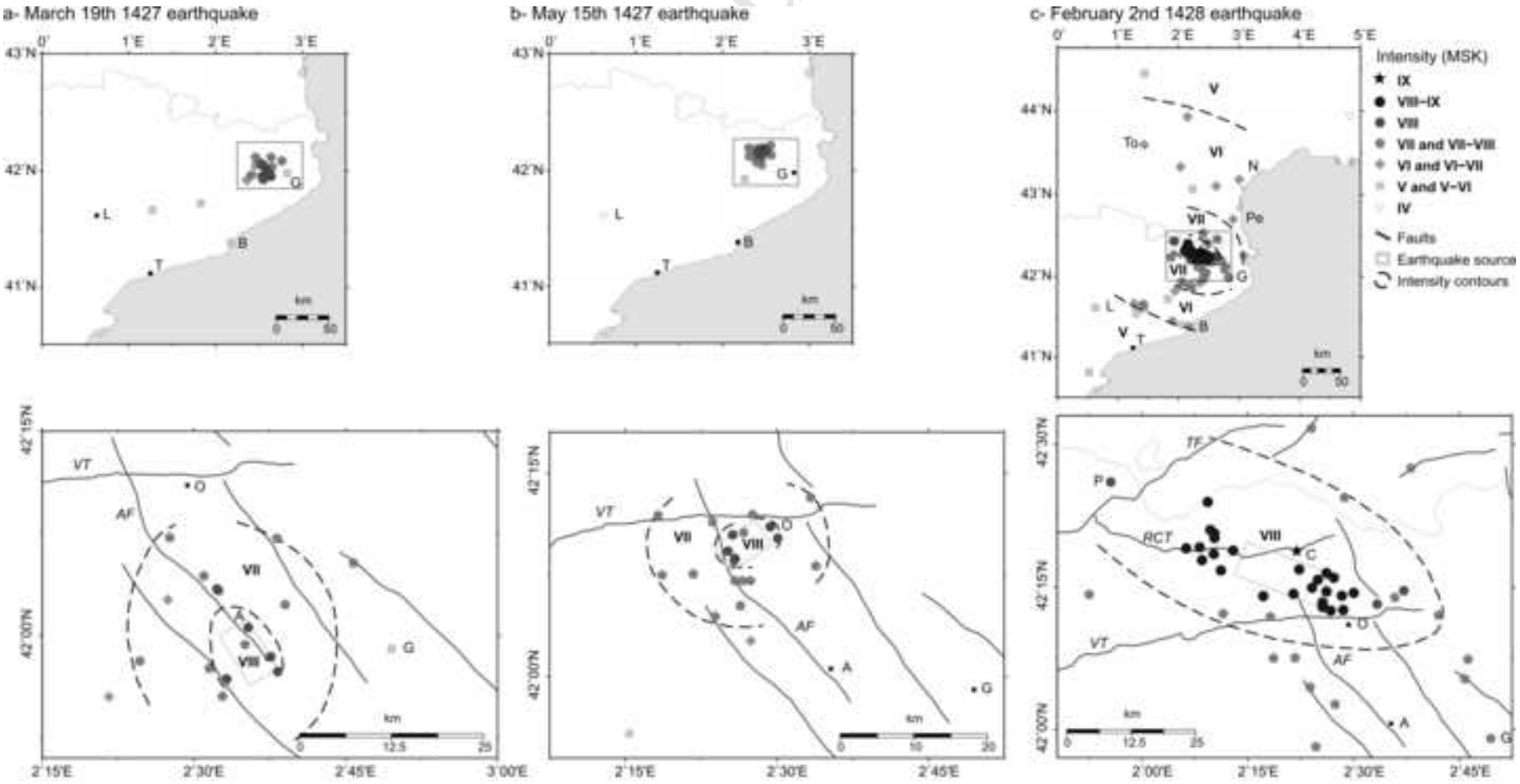

Figure 3 (press publication)

Figure 3 Color
Click here to download high resolution image

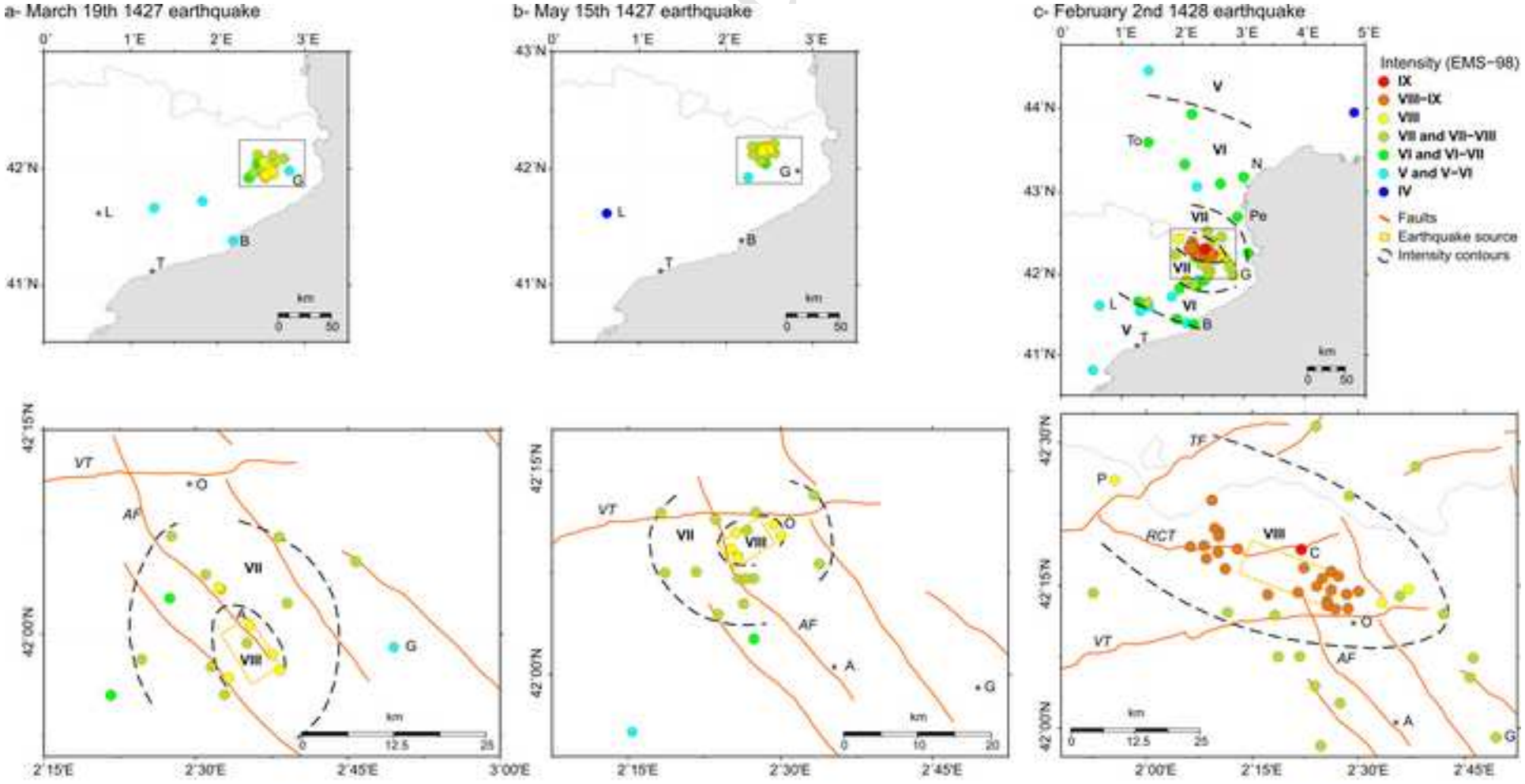

Figure 3 (online publication)

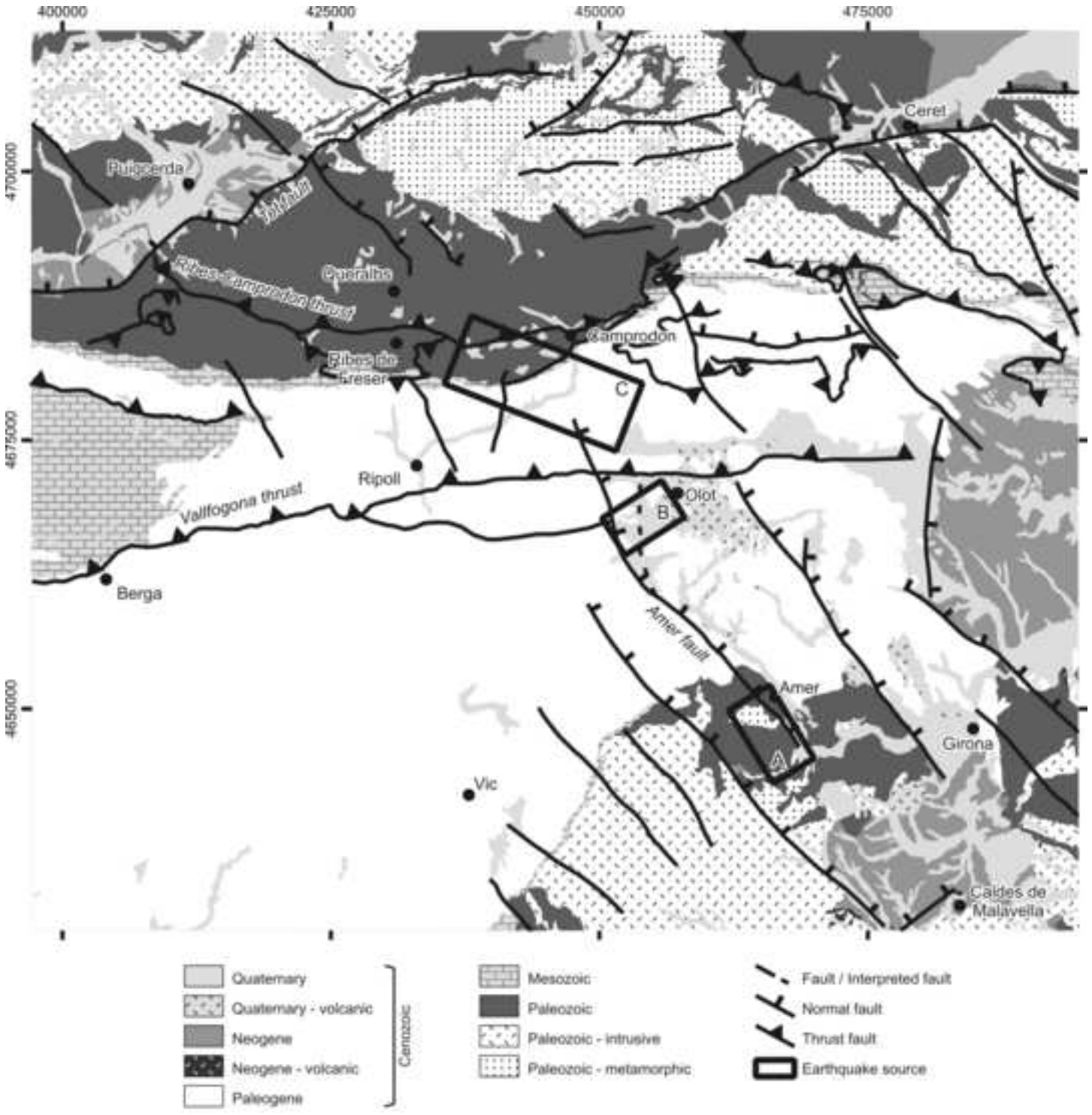

Figure 4 (press publication)

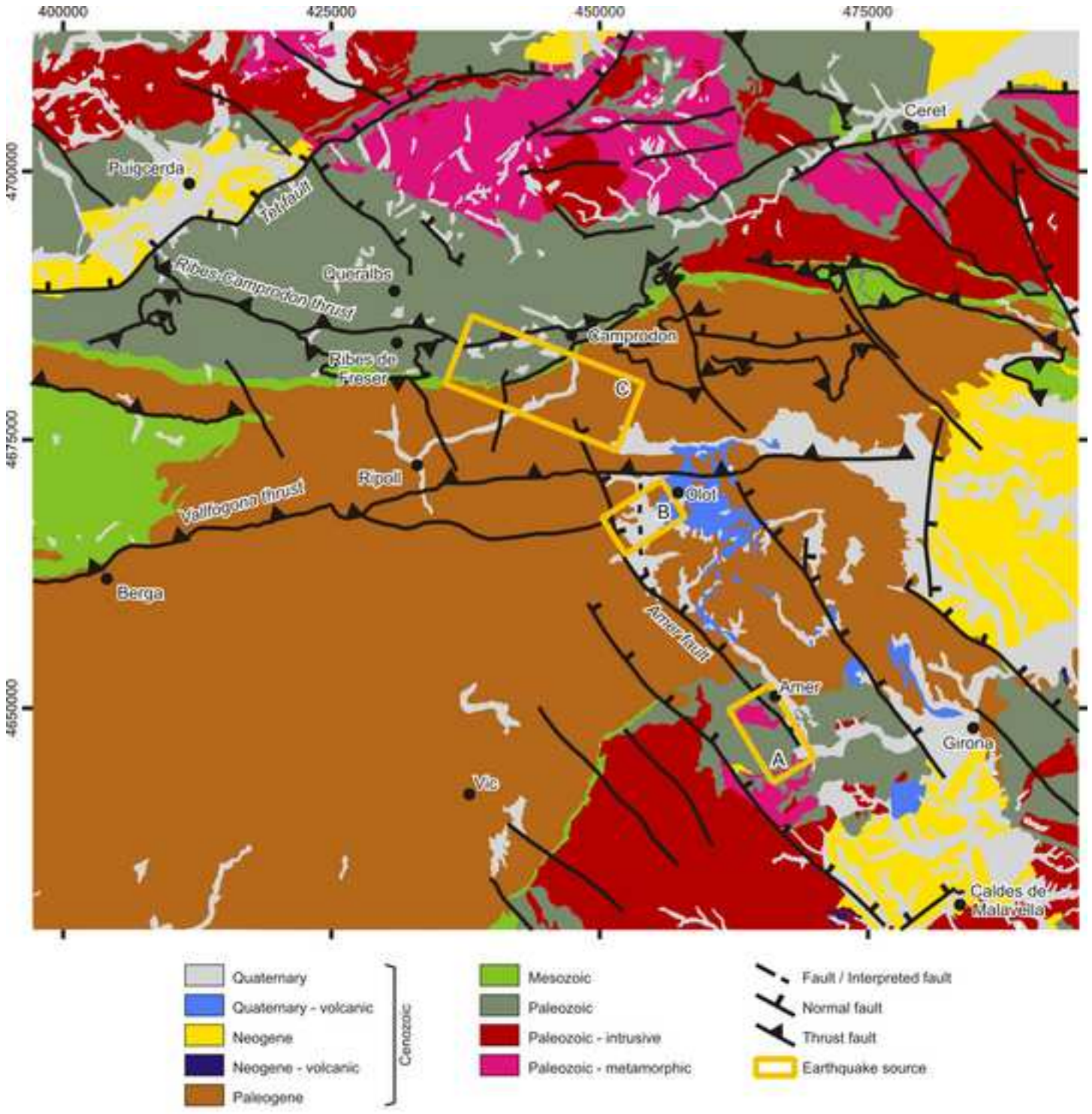

Figure 4 (Online publication)

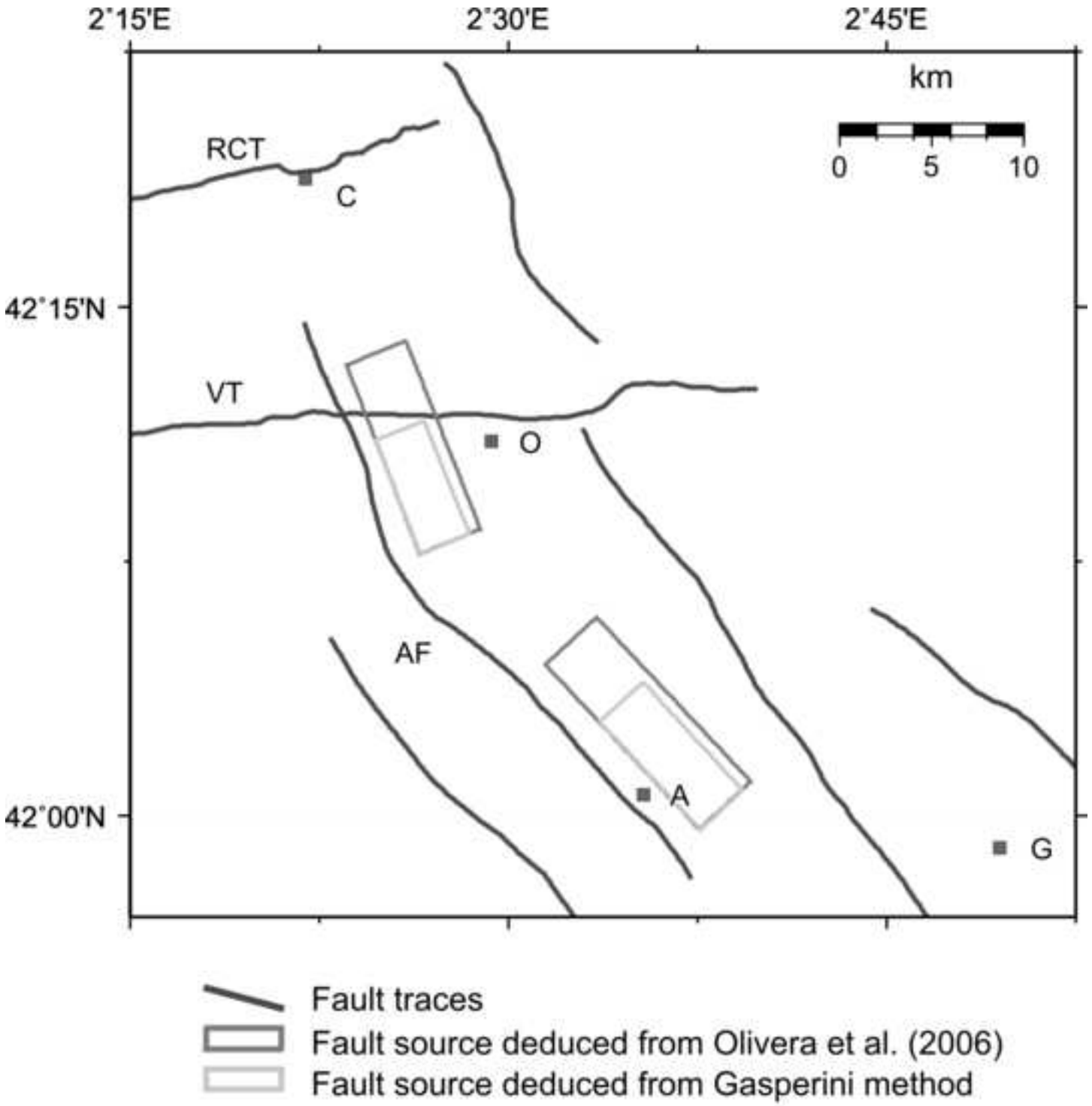

Figure 5 (press publication)

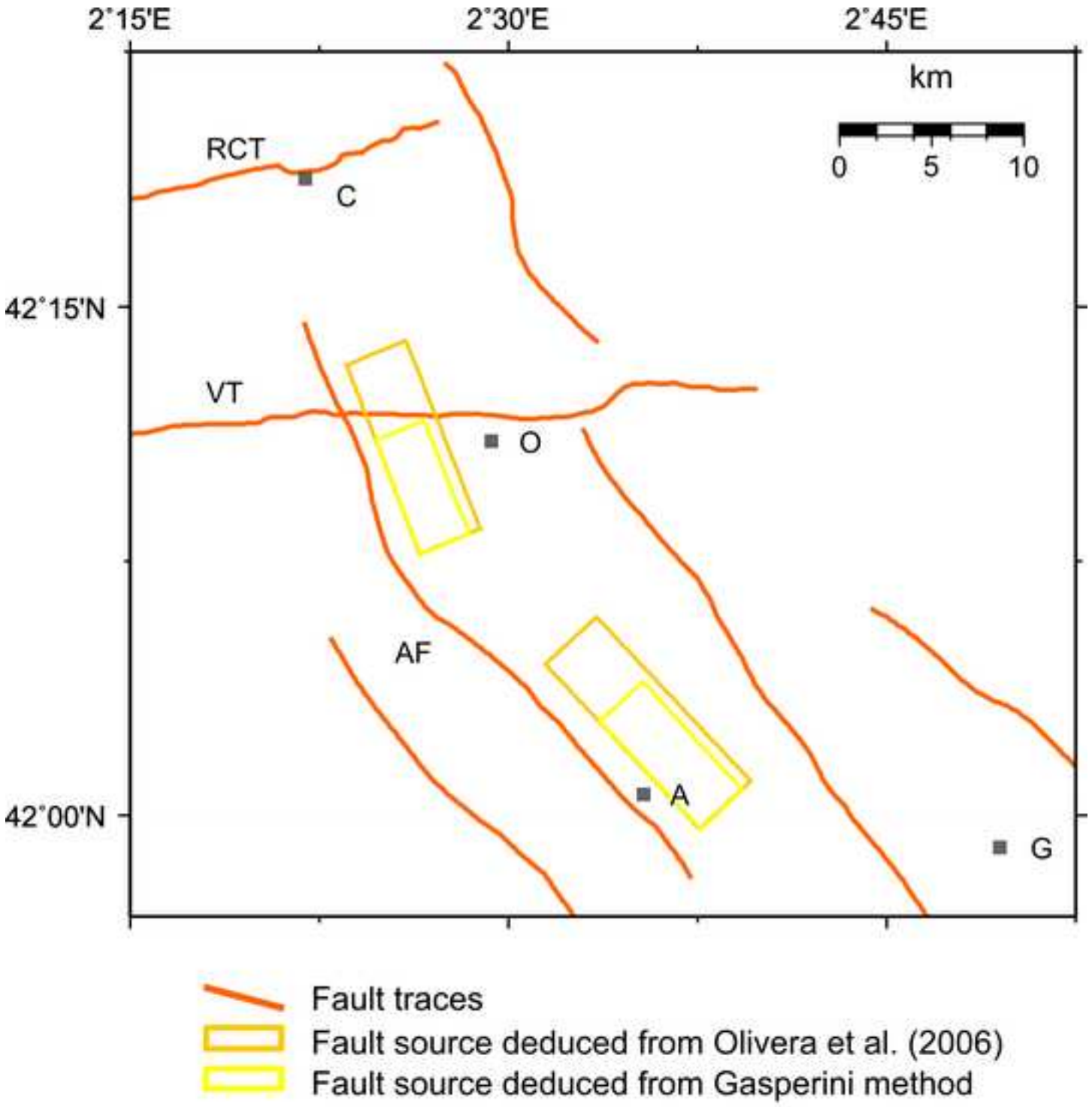

Figure 5 (online publication)

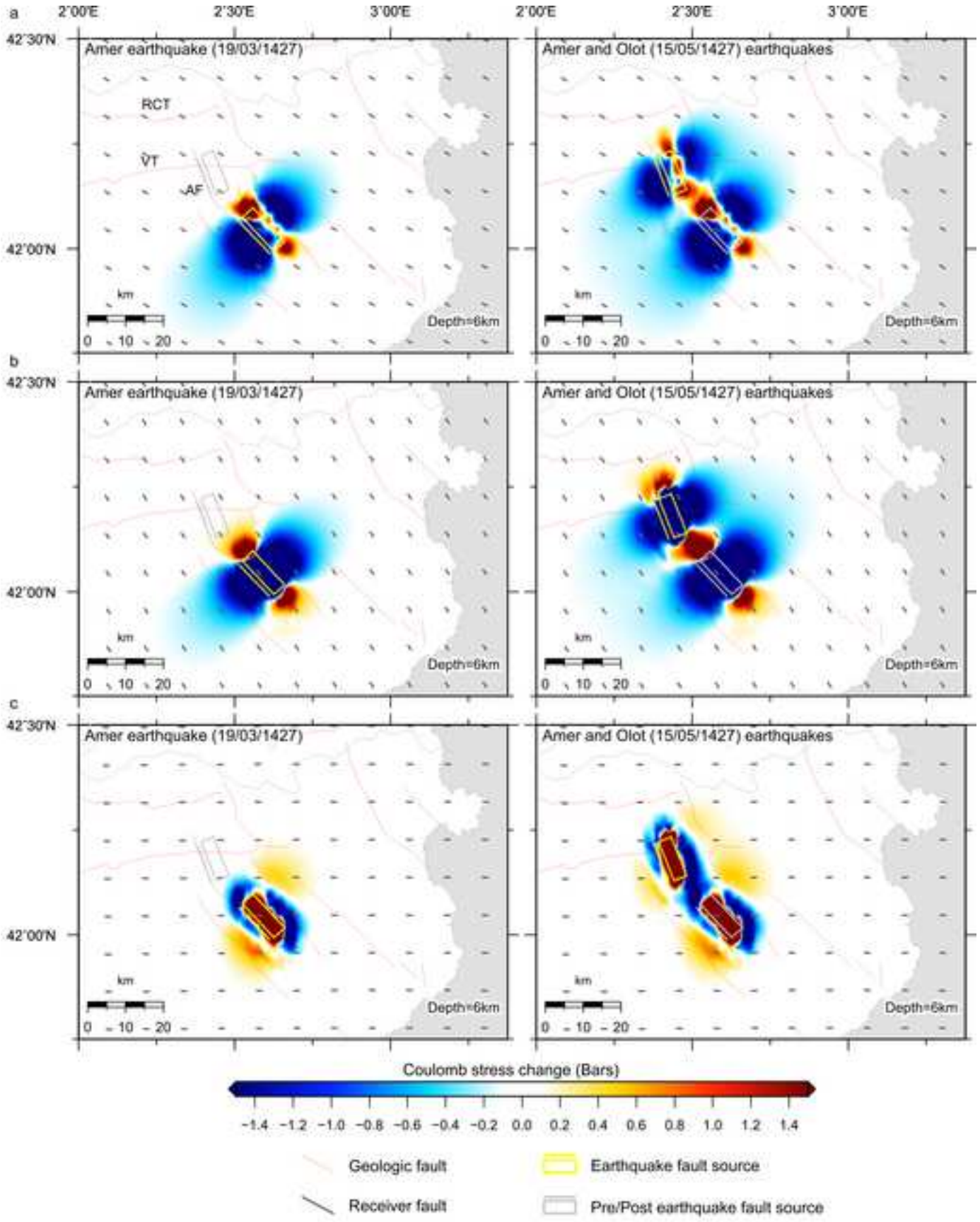
a
b
c
2°00'E
2°30'E
3°00'E
42°30'N
42°00'N
Amer earthquake (19/03/1427)
Amer and Olot (15/05/1427) earthquakes
RCT
VT
AF
km
0 10 20
Depth=6km
Coulomb stress change (Bars)
-1.4 -1.2 -1.0 -0.8 -0.6 -0.4 -0.2 0.0 0.2 0.4 0.6 0.8 1.0 1.2 1.4
Geologic fault
Earthquake fault source
Receiver fault
Pre/Post earthquake fault source

Figure 6

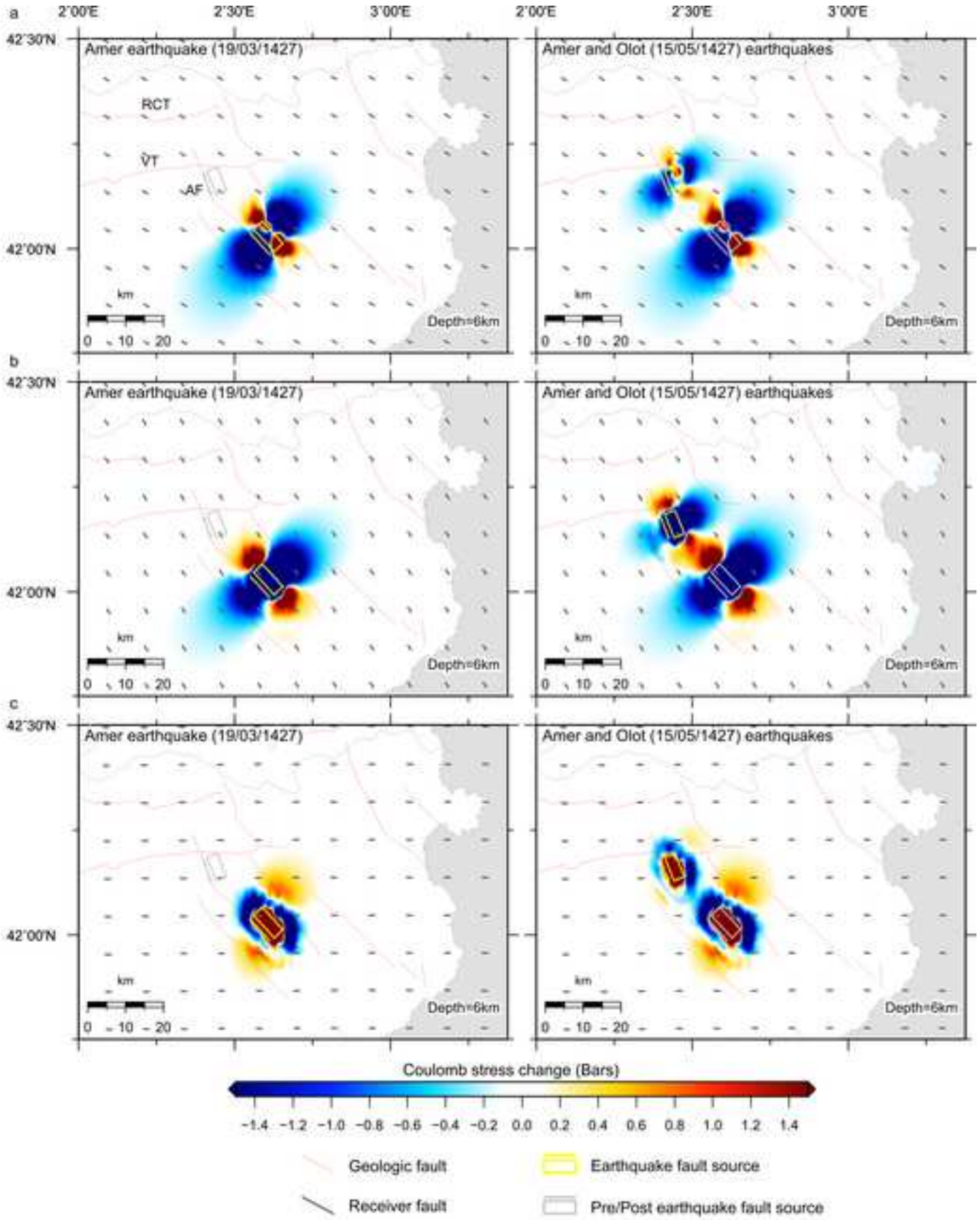
a
b
c
2°00'E
2°30'E
3°00'E
42°30'N
42°00'N
Amer earthquake (19/03/1427)
Amer and Olot (15/05/1427) earthquakes
RCT
VT
AF
km
0 10 20
Depth=6km
Coulomb stress change (Bars)
-1.4 -1.2 -1.0 -0.8 -0.6 -0.4 -0.2 0.0 0.2 0.4 0.6 0.8 1.0 1.2 1.4
Geologic fault
Earthquake fault source
Receiver fault
Pre/Post earthquake fault source

Figure 7

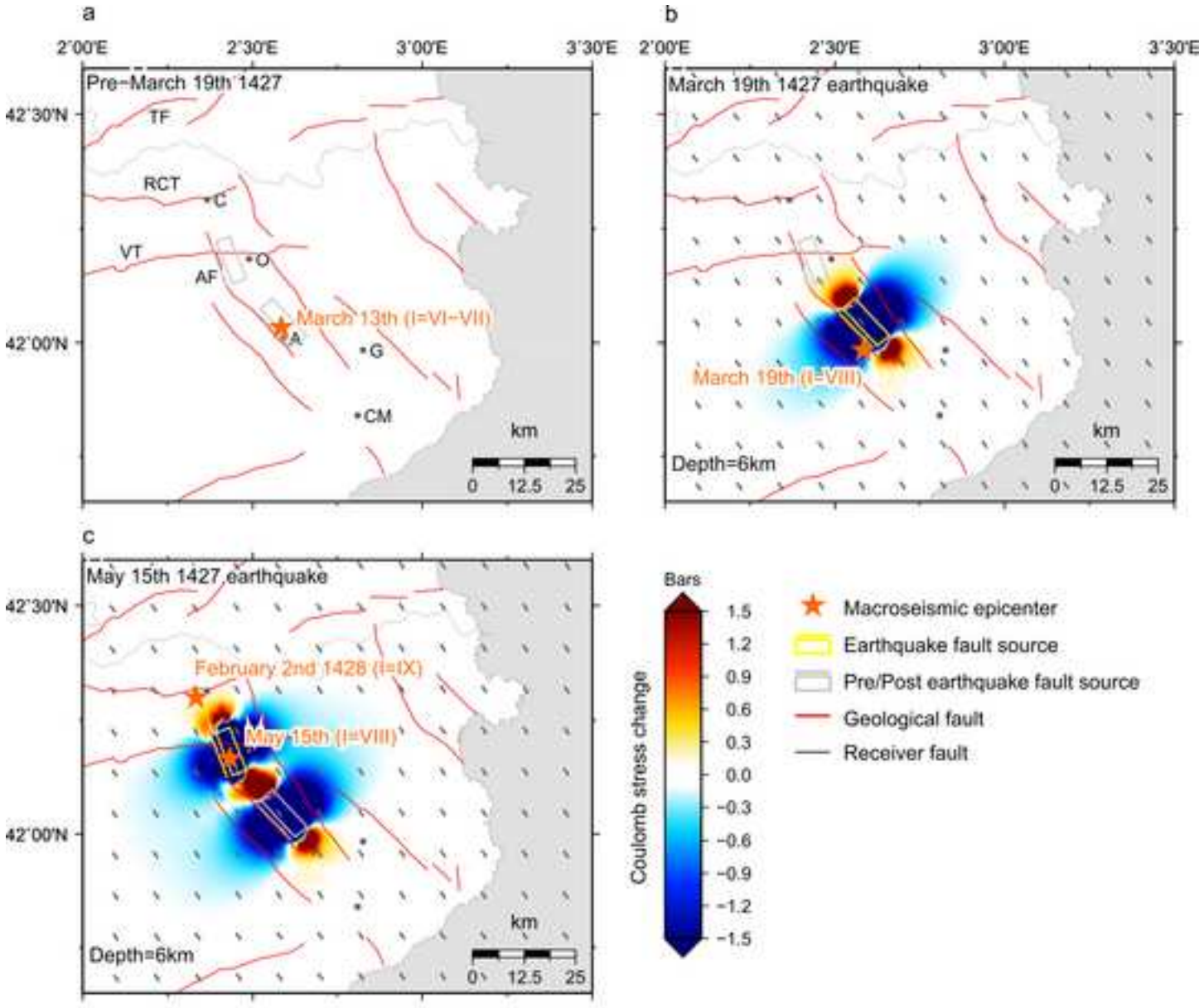
a
2°00'E
2°30'E
3°00'E
3°30'E
42°30'N
42°00'N
Pre-March 19th 1427
TF
RCT
C
VT
O
AF
March 13th (I=VI-VII)
A
G
CM
km
0 12.5 25
b
March 19th 1427 earthquake
March 19th (I=VIII)
Depth=6km
c
May 15th 1427 earthquake
February 2nd 1428 (I=IX)
May 15th (I=VIII)
Bars
Coulomb stress change
1.5
1.2
0.9
0.6
0.3
0.0
-0.3
-0.6
-0.9
-1.2
-1.5
Macroseismic epicenter
Earthquake fault source
Pre/Post earthquake fault source
Geological fault
Receiver fault

Figure 8

Earthquake	Long epicenter	Lat epicenter	Epicentral intensity (EMS-98)	Mw
March 13th 1427	2.5833	42.0333	VI-VII	5.0
March 19th 1427	2.5833	41.9833	VIII	5.9
April 22nd 1427	2.5833	41.9833	VI-VII	5.0
May 15th 1427	2.4333	42.1667	VIII	5.8
June 14th 1427	2.8167	41.8500	VII	5.3
February 2nd 1428	2.3333	42.3000	IX	6.5

Table 1

a. Data from Olivera et al. (2006)

Earthquake	Long epicenter	Lat epicenter	Mw	Area (km^2)[1]	Depth range (km)	Mo (Nm)	Average displacement $(m)^2$
March 19th 1427	2.5833	41.9833	5.9	92.9	2.5 to 9.0	$8.43*10^{17}$	0.3
May 15th 1427	2.4333	42.1667	5.8	76.9	2.5 to 8.5	$6.31*10^{17}$	0.3

b. Data obtained from the application of the Gasperini method

Earthquake	Long epicenter	Lat epicenter	Mw	Area (km^2)	Depth range (km)	Mo $(Nm)^3$	Average displacement $(m)^2$
March 19th 1427	2.6018	41.9945	5.8	50.4	2.5 to 8.0	$6.84*10^{17}$	0.5
May 15th 1427	2.4487	42.1547	5.5	37.6	2.5 to 7.5	$2.43*10^{17}$	0.2

1 Calculated using empirical relationship between magnitude (M) and rupture area (RA) for normal faults log(RA)=-2.87+0.82M (Wells and Coppersmith, 1994)

2 Calculated using $Mo=\mu DA$ (Hanks and Kanamori, 1979)

3 Calculated using $Mw=2/3\ \log_{10}Mo-6.0$ (Nm) (Hanks and Kanamori, 1979)

Table 2